

Exploration of Cyanine Compounds as Selective Inhibitors of Protein Arginine Methyltransferases: Synthesis and Biological Evaluation

Hao Hu,[†] Eric A. Owens,[‡] Hairui Su,[§] Leilei Yan,[†] Andrew Levitz,[‡] Xinyang Zhao,[§] Maged Henary,^{*,‡} and Yujun George Zheng^{*,†}

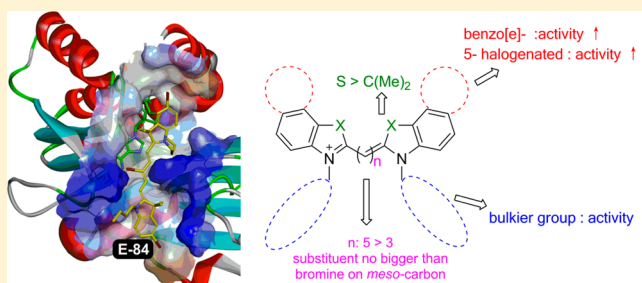
[†]Department of Pharmaceutical and Biomedical Sciences, The University of Georgia, Athens, Georgia 30602, United States

[‡]Department of Chemistry, Center for Diagnostics and Therapeutics, and Center for Biotechnology and Drug Design, Georgia State University, 100 Piedmont Avenue SE, Atlanta, Georgia 30303, United States

[§]Department of Biochemistry and Molecular Genetics, UAB Stem Cell Institute, The University of Alabama at Birmingham, Birmingham, Alabama 35294, United States

S Supporting Information

ABSTRACT: Protein arginine methyltransferase 1 (PRMT1) is involved in many biological activities, such as gene transcription, signal transduction, and RNA processing. Overexpression of PRMT1 is related to cardiovascular diseases, kidney diseases, and cancers; therefore, selective PRMT1 inhibitors serve as chemical probes to investigate the biological function of PRMT1 and drug candidates for disease treatment. Our previous work found trimethine cyanine compounds that effectively inhibit PRMT1 activity. In our present study, we systematically investigated the structure–activity relationship of cyanine structures. A pentamethine compound, E-84 (compound **50**), showed inhibition on PRMT1 at the micromolar level and 6- to 25-fold selectivity over CARM1, PRMT5, and PRMT8. The cellular activity suggests that compound **50** permeated the cellular membrane, inhibited cellular PRMT1 activity, and blocked leukemia cell proliferation. Additionally, our molecular docking study suggested compound **50** might act by occupying the cofactor binding site, which provided a roadmap to guide further optimization of this lead compound.



INTRODUCTION

Protein arginine methylation is a prevalent posttranslational modification that is mediated by protein arginine methyltransferases (PRMTs).^{1–5} During this process the methyl group of cofactor S-adenosylmethionine (SAM) is transferred to substrate arginine and SAM is converted to S-adenosylhomocysteine (SAH). PRMTs can be divided into three types (types I, II, and III) according to the degree and position of methylation.^{6–8} Type I converts arginine into monomethylarginine (MMA) and further into asymmetric dimethylarginine (ADMA). Type II produces MMA and symmetric dimethylarginine (SDMA), while type III can only generate MMA. Among them, PRMT1 is a type I methyltransferase that accounts for over 80% arginine methylation in vivo.⁹ PRMT1 plays important roles in many biological processing,¹⁰ such as gene transcription, signal transduction, RNA processing, and DNA repair.^{3,11–14} Moreover, overexpression of PRMT1 is reported to be related to cardiovascular diseases,^{15–18} kidney disease,^{19–22} and many kinds of cancers, e.g., prostate cancer,²³ breast cancer,²⁴ and leukemia.^{25,26} Therefore, the development of PRMT1-selective inhibitors will not only benefit the investigation of the function and biological roles of PRMT1 but also provide a therapeutic strategy for these diseases.

So far, much work has been done to develop selective PRMT inhibitors, which could be structurally divided into two classes.

The first class comprises peptide derivatives.^{27–29} The underlying rationale is that because the SAM-binding pocket of PRMTs is highly conserved, it might be difficult to discriminate between isozymes with SAM analogs.^{4,7,30,31} Instead, inhibitors containing specific substrate sequences might offer enhanced selectivity. Though these substrate analogs indeed gained some extra inhibitory activity, there is no remarkable improvement for the selectivity. Since some of them act as substrate inhibitors²⁷ or irreversible inhibitors²⁸ and the molecular size of peptides are relatively large, these peptide inhibitors are more like PRMT1 function dissecting tools rather than ideal drug candidates. The second class inhibitors are organic small molecules, which are normally obtained from random or target-based screening, such as AMI-1, stilbamidine, allantodapsone, RM6S, and SAM derivatives (Figure 1).^{32–35} A few structurally related inhibitors, including the diamidine compound DB75 recently reported by our group, are rationally investigated.^{36–43} On one hand, having diverse structures provided more opportunities for exploration of potential inhibitors; conversely, the structural dissimilarity from SAM or substrate makes it hard to generalize the ideal pharmacophores and predict the activity.

Received: September 21, 2014

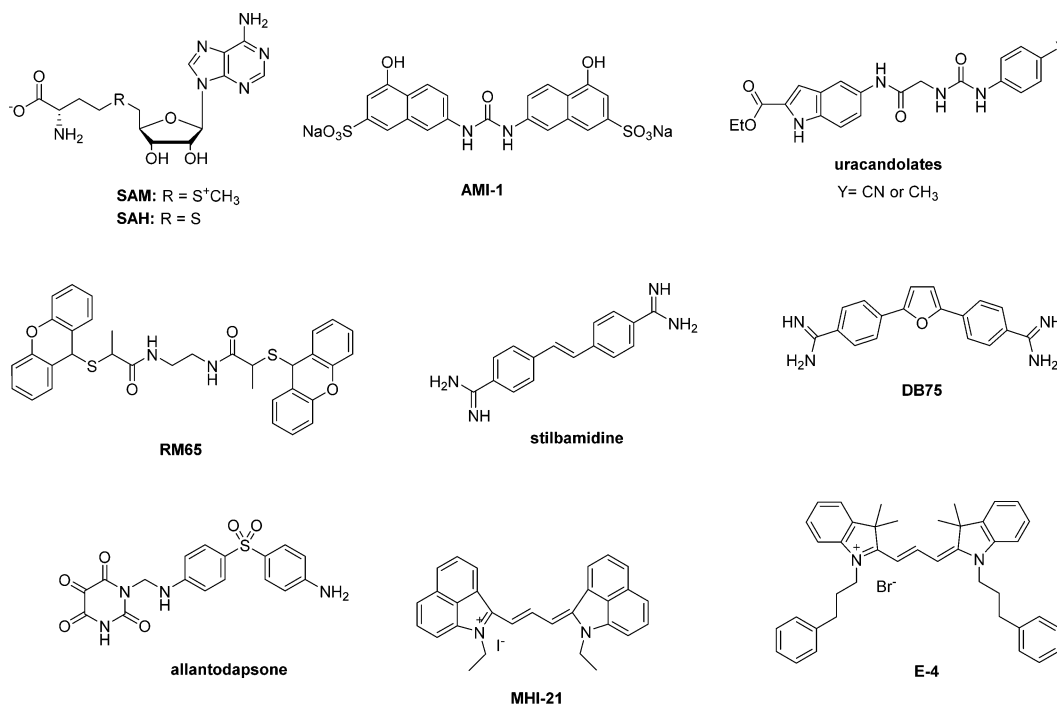
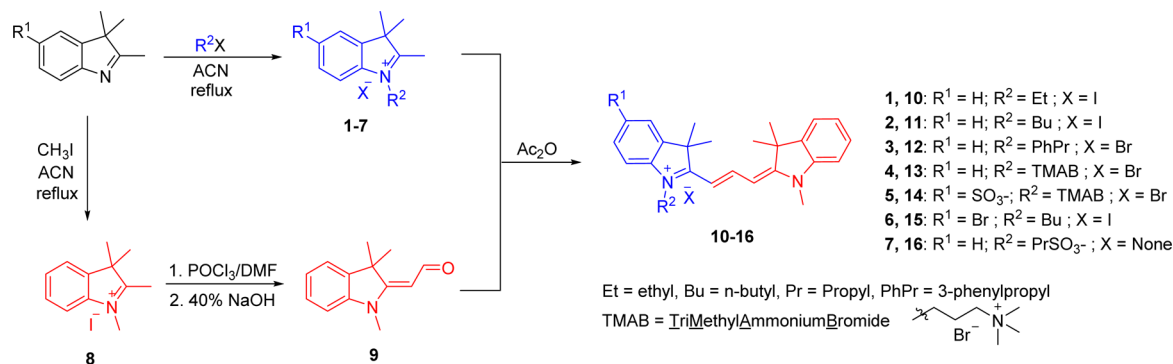


Figure 1. Structures of SAM, SAH, and reported PRMT inhibitors including AMI-1, uracandolates, RM65, stilbamidine, DB75, allantodapsone, MHI-21, and E-4.

Scheme 1. Synthetic Route for the Preparation of 3,3-Dimethylindolenine Based Unsymmetric Trimethine Cyanines 10–16



For example, some derivatives of AMI-1, dubbed as “uracandolates”, turned out to be a CARM1/PRMT4 activity enhancer.⁴⁴ A culmination of these effects has prevented great strides to be made toward the development of selective PRMT1 inhibitors.

Cyanine dyes possess two nitrogen containing heterocycles that are connected by an electron deficient conjugated methine bridge that provides an important characteristic of carbocyanines—their red-shifted absorption and fluorescence wavelengths.^{45–47} Through various synthetic methods, the absorption and fluorescence of these compounds can be tuned from 400 to 1000 nm. Cyanine–biomolecule interactions can be easily quantitated spectrophotometrically through the relative changes in the absorption or emission spectra.

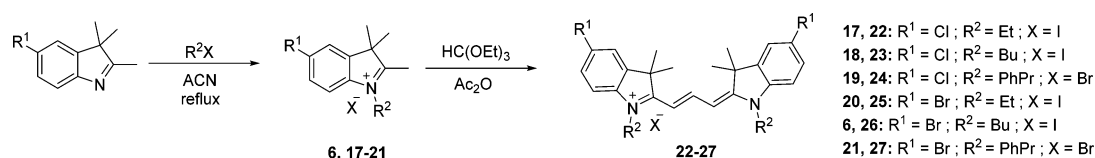
Our previous effort was put into discovering potential PRMT1 inhibitors from a set of trimethine cyanines, among which compound MHI-21 (Figure 1) was shown to possess good potency with moderate selectivity for PRMT1 over other PRMTs.⁴⁸ Because of the intriguing results and the unique spectroscopic properties of the cyanine structures, we decided to finely tune their binding properties and create diversified

compounds for PRMT inhibition. Having carefully checked the previous results, we chose compound E-4 (Figure 1) as an appealing structure for further exploration because it (1) showed promising inhibitory activity and (2) contained a less synthetically complex aromatic ring system which likely increases the potential for further modification. Herein, we discuss a systematic structure–activity relationship (SAR) for E-4-like compounds and identified compound **50** as a potent inhibitor with selectivity for PRMT1 over CARM1/PRMT4, PRMT5, and PRMT8. Besides, the cellular activity supported that **50** can permeate cell membrane, inhibit intracellular PRMT1 activity, and block leukemia cell proliferation. Also, ligand–enzyme interactions were studied in detail by molecular docking to understand the SAR and offer structural clues for further optimization.

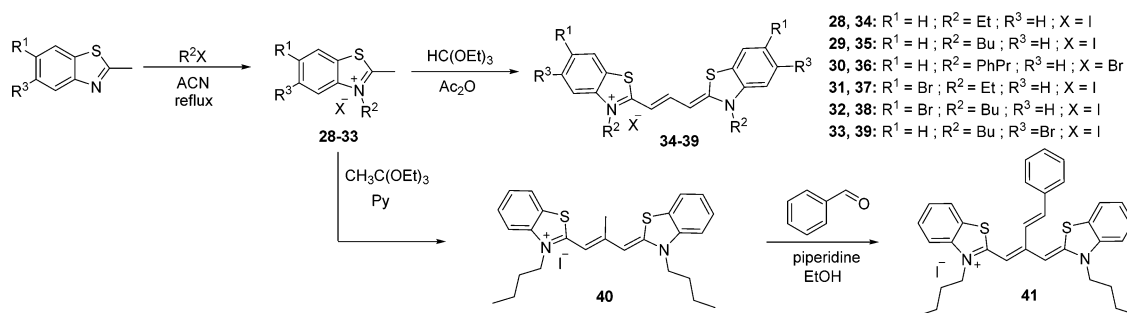
RESULTS AND DISCUSSION

1. Chemistry and Synthesis. In order to thoroughly investigate the structure–activity relationship of the cyanine PRMT inhibiting agents, we prepared a series of tri- and

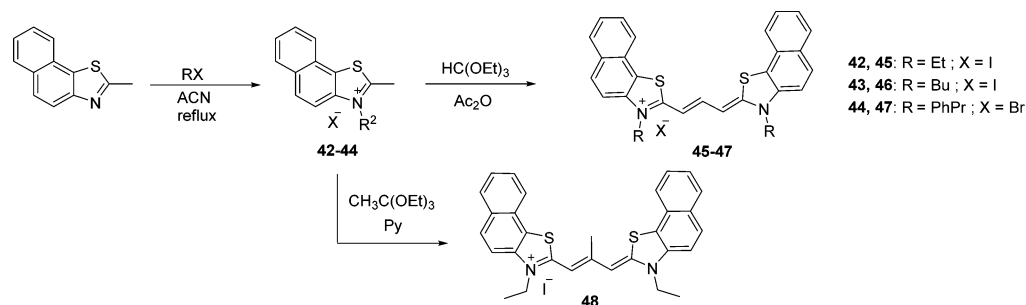
Scheme 2. Synthetic Route for the Preparation of 3,3-Dimethylindolenine Based Symmetric Trimethine Cyanine PRMT Inhibiting Agents 22–27



Scheme 3. Synthetic Route for the Preparation of Benzothiazole-Based Trimethine Cyanines without (34–39) and with (40 and 41) *meso*-Modification



Scheme 4. Synthetic Route for the Preparation of Naphthothiazole-Based Trimethine Cyanines without (45–47) and with (48) *meso*-Modification



pentamethine cyanines based on previously reported cyanine inhibitors to augment the potency of inhibitory properties. We first used an effective route toward the preparation of asymmetric cyanines maintaining a methyl group on one side of the inhibitors. The first step in the synthesis requires the quaternization of the 2,3,3-trimethylindolenine heterocyclic portion that affords compounds 1–7. In parallel, this heterocycle is methylated and subjected to Vilsmeier formylation followed by basic hydrolysis to afford the aldehyde 9. This aldehyde reacts effectively with individual 1–7 to yield the final asymmetric compounds 10–16 (Scheme 1). Several solvents including acetic anhydride, acetonitrile, pyridine, and ethanol were used for the development of the synthetic protocol for the final compound preparation step, and acetic anhydride was found to perform the transformation with the highest purity.

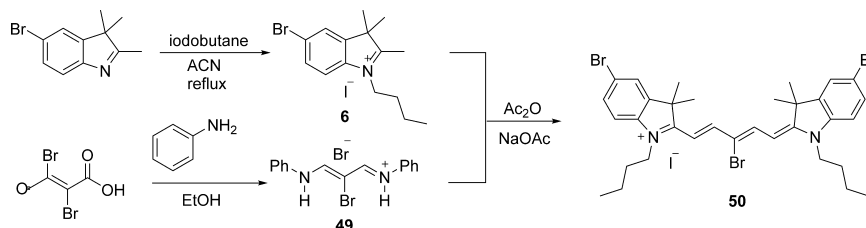
Symmetric PRMT-inhibiting cyanines previously synthesized were moderately effective without heterocyclic modification. To potentially increase inhibitory efficacy, we have incorporated halogens on the phenyl ring of such inhibitors. The synthetic route began with Fischer indole synthesis and methylation which afforded the indolenine heterocyclic derivatives 6 and 17–21. These quaternary salts were then allowed to react with triethyl orthoformate, which yielded the symmetric compounds 22–27 (Scheme 2).

Similar chemistry was applied to the preparation of analogous benzothiazole-based cyanine compounds 34–39 with

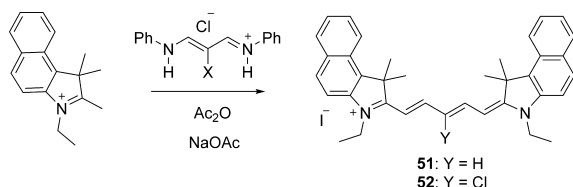
different positions of halogen incorporation. Since benzothiazoles have been reported to bind the minor groove of duplex DNA,^{49–51} we incorporated a steric restraint toward preventing this interaction. Reacting benzothiazole salts 28–33 with triethyl orthoacetate afforded the cyanine compounds featuring a methyl group in the central position of the polymethine bridge (Scheme 3). The delocalized cation allows this central methyl group to be acidic; reacting at this position in the presence of pyridine with a corresponding aldehyde affords the central modification of compound 41. Similar methyl-incorporating chemistry cannot be applied to the dimethylindolenine core because of steric interactions with the dimethyl groups. Identical reaction conditions were applied to the naphthothiazole heterocyclic compound shown in Scheme 4.

In order to draw conclusions about the length of the polymethine bridge, we elongated the structure one vinylene unit ($-\text{CH}=\text{CH}-$), comparing trimethine compound 26 to pentamethine compound 50. The route to 50 began with the formation of brominated salt 6. Separately, reacting muco-bromic acid with a warm ethanolic solution of aniline afforded the polymethine linking precursor 49. These two intermediates reacted under basic conditions in acetic anhydride to yield 50 (Scheme 5).

In addition, using similar synthetic methodology, we prepared the pentamethine analogs shown in Scheme 6 for direct

Scheme 5. Synthetic Route for the Preparation of Brominated Pentamethine Cyanine Dye 50 with an *N*-Butyl Substituent

Scheme 6. Synthetic Route for the Preparation of Benz[e]indolenine Pentamethine Cyanine Dyes 51–54



polymethine length comparison to our previously published trimethine compounds.

2. Inhibitory Activity of the New Cyanine Compounds for PRMT1 and SAR Analysis. Scintillation proximity assay⁵² was used to test inhibitory activity of each new compound on PRMT1 inhibition. Briefly, inhibitor was incubated with [³H]-labeled SAM (S-adenosylmethionine) and H4(1–20)-BTN peptide (a biotinylated 20-amino-acid peptide from H4 histone N-terminus) before initiating the reaction by adding recombinant His6x-PRMT1. The inhibition ratio was used to assess the potency of each inhibitor against PRMT1 activity (Tables 1–3). It should be noted that all the enzyme reactions in this work were controlled under initial rate condition, where the peptide methylation was linear with time.

The compound represented by E-4 can be considered as a “dimer”: a polymethine spacer connecting two identical “monomers”. Each “monomer” can be further divided into an aromatic ring (head) and an *N*-substituted side chain (tail). The IC₅₀ values were reported⁴⁸ for indolium-headed E-14, E-6, and E-4 and benz[e]indolium-headed E-5, E-18, and E-8 (for structures, see Table 1). Since the potency can vary under different assay conditions, we began by retesting the PRMT1 inhibition for these compounds at 10 μ M under the same experimental condition to make sure the data are comparable with each other. In consistence with our previous results, we found that when the “head” or “tail” became bulkier or more hydrophobic, the activity was improved. For example, the bigger-headed E-5 (27% at 10 μ M), E-18 (91% at 10 μ M), and E-8 (100% at 10 μ M) showed superior activities compared with E-14 (4% at 10 μ M), E-6 (no inhibition, N.I., at 10 μ M), and E-4 (41% at 10 μ M), respectively. Also, E-4 and E-8, which both have a phenylpropyl group as the “tail”, showed better inhibition than those with the same “heads” but shorter “tails” (E-14 and E-6, and E-5 and E-18, respectively).

SAR for Indolium-Based Cyanines (Series 1). The initial investigation was focused on the indolium derivatives (series 1, see Table 1). To elucidate the impact of symmetry on activity, general “monomers” (1–3) and simple asymmetrical indolium cyanines (10–16), where modifications were introduced into just one head, were synthesized. It turned out compounds 1–3

exhibited no inhibition even at 90 μ M, indicating the double-headed structure is essential for maintaining activity. As expected, the activities increased along with the structural symmetry. This can be seen by comparing 10 (9% at 30 μ M) vs E-14 (42% at 30 μ M), 11 (32% at 30 μ M) vs E-6 (48% at 30 μ M), and 12 (35% at 10 μ M) vs E-4 (41% at 10 μ M). Interestingly, the structural symmetry seems not as important as the “tail” hydrophobicity, as can be seen in that compound 12 (35% at 10 μ M) with a bulky phenylpropyl tail is a better inhibitor than E-6 and E-14 with shorter tails.

Then further modifications were introduced on both the “head” and “tail” of the dimer structures. The addition of either negative or positive charged groups on the end of the butyl “tail” adversely affected the inhibitory activity. For example, at 10 μ M, charged compounds 13 (2%) and 16 (N.I.) showed weaker or no activity compared with compounds 11 (8%) containing a neutral butyl tail. As to the modification on the “nude (unsubstituted) head”, the incorporation of 5-sulfonate group abolished activity by comparing 13 and 14 (N.I.). However, 5-bromination brought the inhibition rate up to 36% of 15 from 8% of 11, which is reasonable because halogen substituents predominately prevail in drug development as a hydrophobic group, Lewis acid, or forming “halogen bond” in ligand–protein interactions.^{53,54}

On the basis of the SAR mentioned above, as well as the fact that many PRMT1 inhibitors are reported to contain symmetric structures,^{32,34,35,38,39} we prepared symmetric 5,5′-dichloro- and 5,5′-dibromoindolium cyanines (compounds 22–27). Again, as the “tail” became longer and bulkier, as seen from 22 through 24 and from 25 through 27, the potency was enhanced. Compared to the prototypes, all halogenated compounds gained extra activity. For example, 10 μ M phenylpropyl derivatives 24 and 27 even displayed about 100% inhibition on PRMT1, compared with E-4. It seems bromine played a slightly (if any) better role than chlorine on potency enhancement.

SAR for Thiazolium-Based Cyanines (Series 2). The second series of compounds (Series 2, see Table 2) were obtained by replacement of the indolium-based cyanines with a benzothiazole ring containing a sulfur atom. It turned out this subtle change was efficacious for the benzothiazoliums, especially for those with low potency. For example, compounds 35 and 37 showed inhibition up to 79% and 88% at the concentration of 10 μ M, in contrast to the corresponding indolium species E-6 (N.I.) and compound 25 (11%), respectively. Besides, the activity was retained when the bromine atom on C-6 (38, 93%) was moved to C-5 (39, 91%).

The success of the 3,3-dimethyl-to-sulfur alteration strategy, coupled with the “bulkier head, better inhibitor” SAR, prompted us to generate naphthothiazoliums 45–47. As expected, these compounds indeed turned out to be satisfactory inhibitors to PRMT1, though they failed to exhibit further improvement on

Table 1. Inhibition and IC₅₀ for Indolium-Related Compounds

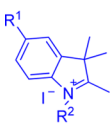
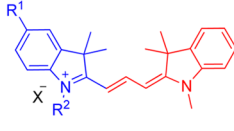
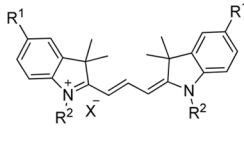
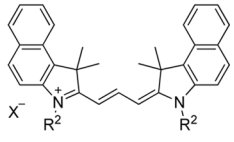

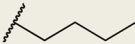
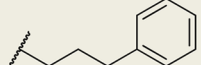
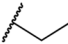
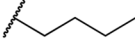
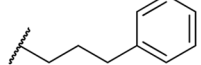
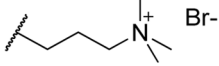
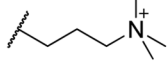
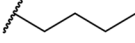
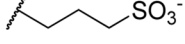
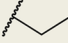
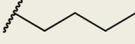
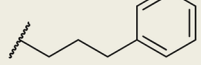
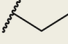
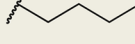
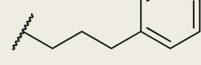
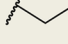
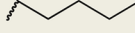
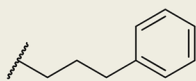
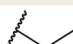
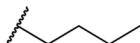
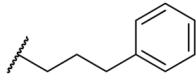
<div>     </div>									
Cmpd# ^a	Name	R1	R2	X	Inhibition (10 μM)	Inhibition (30 μM)	Inhibition (90 μM)	IC ₅₀ (sd) ^b	n _H (sd)
1	E-14S	H		I ⁻	N.I. ^c	N.I.	N.I.		
2	E-6S	H		I ⁻	N.I.	N.I.	N.I.		
3	E-4S	H		Br ⁻	N.I.	N.I.	80.00%		
10	AL-34	H		I ⁻	N.I.	9 %	41%		
11	AL-36	H		I ⁻	8%	32%	79%		
12	AL-35	H		Br ⁻	35%	96%	101.00%		
13	AL-14	H		Br ⁻	2%				
14	AL-16	SO ₃ ⁻		Br ⁻	N.I.				
15	AL-46	Br		I ⁻	36%				
16	AL-18	H			N.I.				
	E-14	H		I ⁻	4%	42%	60.60%		
	E-6	H		I ⁻	N.I.	48%	91%		
	E-4	H		Br ⁻	41%	101.00%	100%		
22	E-96	Cl		I ⁻	7%				
23	E-97	Cl		I ⁻	34%				
24	E-98	Cl		I ⁻	100%			1.15 (0.038)	6.26 (0.95)
25	T-21	Br		I ⁻	11%				
26	E-86	Br		I ⁻	48%				

Table 1. continued

Cmpd# ^a	Name	R1	R2	X	Inhibition (10 μ M)	Inhibition (30 μ M)	Inhibition (90 μ M)	IC ₅₀ (sd) ^b	n _H (sd)
27	T-22	Br		I ⁻	101%			1.25 (0.066)	6.53 (1.53)
	E-5			I ⁻	27%				
	E-18			I ⁻	91%			2.56 (0.28)	3.44 (1.12)
	E-8			Br ⁻	100%			0.61 (0.025)	3.52 (0.54)
	SAH							0.42 (0.015)	1.03 (0.04)

^aCmpd# = compound number. ^bsd = standard deviation. ^cN.I. = no inhibition.

activity comparing to the benzothiazoliums **34–35** and the benzoindoliums **E-5**, **E-18**, and **E-8**.

Meanwhile, it is worth noting that the halogen substitutions on the aromatic ring enhanced the activity by comparing **37** (88%) vs **34** (46%), **38** (93%) vs **35** (79%), and bulkier “tails” in these thiazolium-based compounds exhibited the better activities (comparing **34–36** or **45–47**). These trends are the same as in series 1, indicating these two series of compounds probably have the same binding mode to PRMT1.

Modifications of the Spacers of Indolium Derivatives (Series 3). So far, the thiazolium-based structures (series 2) seem to be more promising for further study than the dimethylindolium derivatives (series 1). Nevertheless, some benzothiazolium cyanines have also been reported to bind the minor groove of *dsDNA*.^{49–51} On the contrary, the dimethylindolium lost the double strand DNA (*dsDNA*) binding ability probably because of steric hindrance in ligand–DNA interaction caused by the dimethyl moiety.^{55,56}

From this perspective, we assumed that the steric hindrance on spacer of the thiazole-containing cyanine would also impair the interaction with *dsDNA*. Therefore, methyl and styryl groups were introduced onto the *meso*-carbon in the trimethine spacer. For benzothiazoliums, substitution at the central methine carbon with methyl group (**40**, 77%) retained the activity of the parent molecule (**35**, 79%), but substitution with more bulky group styrene (**41**, 48%) decreased the potency. As for the naphthothiazoliums, methylation at the central methine carbon enhanced the potency, as indicated by comparing **45** (40%) and **48** (90%). These results held promise for developing the thiazole-based cyanine structures into PRMT-specific inhibitors rather than *dsDNA* binders.

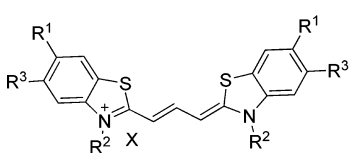
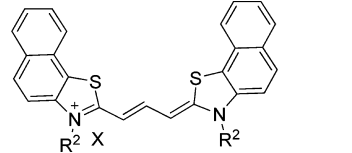

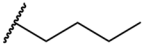
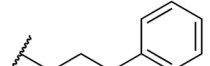
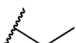
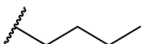
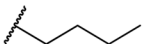
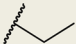
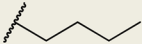
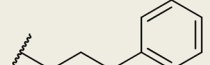
On the other hand, because the dimethylindolium-based structure has the innate property to reject binding with *dsDNA*, it was subjected to further modifications including elongation of spacer and addition of halogen atom on *meso*-carbon (Table 3). Since it was easy to tell how modifications affected the potency for those with moderate inhibitory activity, compound **26** (48%) and **E-5** (27%) were chosen as “parent” compounds. The elevated inhibition ratio of compounds **50** (96%) and **52**

(69%) demonstrated that longer chain could result in better activity, perhaps because the gained flexibility renders the molecule a better binding conformation or the longer distance between two “heads” is more favored by the binding pocket. Besides, the nonchlorinated compound **51** (89%) has better activity than **52**. Further development of **51** and **52** by changing “tail” to phenylpropyl group yielded **53** and **54**, respectively. The better activity of **54** (96%) than **53** (70%) indicates that the effect of spacer chlorination might not be uniform, likely because compounds with different “tails” have slight differences regarding to the binding poses. On the basis of IC₅₀ values which are in range of less than 3-fold, halogen-substitution on the central methine carbon subtly affected the activity of these cyanine compounds in PRMT1 inhibition.

3. Specificity Profiling. One of our goals is to obtain selective inhibitors for PRMT1 over other PRMT isoforms. So several potent inhibitors were picked out and further evaluated against different PRMTs. First, IC₅₀ values against PRMT1 for those with inhibition higher than 90% at 10 μ M were determined to identify accurate potencies. The fractional activities were plotted with the concentrations and fitted to the Hill equation. Generally speaking, the result was well matched with that from the previous screening. Unexpectedly, the most potent inhibitor is the benzoindolium **E-8** (0.61 μ M), which is about 5-fold more potent than its naphthothiazolium counterpart **47** (3.05 μ M).

For each enzyme assay for the other PRMT members, the concentrations of [³H]SAM and the substrate were set around respective K_m values so that the resulting IC₅₀ values of the same compound can be compared between different PRMTs. As shown in Figure 2 (and Table S1), indolium-based compounds **E-8** and **24** were very potent for blocking the activities of all the tested PRMTs. **E-8** only showed very minor specificity for PRMT1 (0.61 μ M) over PRMT5 (1.4 μ M) and PRMT8 (1.74 μ M), while compound **24** possesses no selectivity. The thiazolium compound **39** exhibited moderate (3- to 4-fold) PRMT1 (2.03 μ M) selectivity over CARM1 (7.23 μ M) and PRMT5 (8.36 μ M). Compared to it, compound **47** showed even lower (about 2-fold) selectivity to the same set of enzymes

Table 2. Inhibition and IC₅₀ for Thiazolium-Based Compounds

									
		34-39				45-47			
Cmpd# ^a	name	R1	R2	R3	X	Inhibition (10 μM)	IC ₅₀ (sd ^b)	n _H (sd)	
34	AH-11	H		H	I ⁻	46%			
35	AL-56	H		H	I ⁻	79%			
36	AL-58	H		H	Br ⁻	76%			
37	AH-25	Br		H	I ⁻	88%	6.43 (0.12)	5.88 (0.63)	
38	AL-62	Br		H	I ⁻	93%	2.67 (0.080)	3.12 (0.28)	
39	AL-66	H		Br	I ⁻	91%	2.03(0.028)	2.7 (0.09)	
45	AL-77				I ⁻	40%			
46	AL-70				I ⁻	99%	4.00 (0.04)	6.84 (0.45)	
47	AL-83				I ⁻	100%	3.05 (0.23)	2.78 (0.56)	

^aCmpd# = compound number. ^bsd = standard deviation.

(3.05 μM for PRMT1, 5.8 μM for CARM1, and 7.04 μM for PRMT5), but its inhibitory activity on PRMT1 is more than 9-fold higher than on PRMT8 (28.4 μM). As for the longer-spacer compound **50**, it displays more than 6-, 10-, and 25-fold selectivity for PRMT1 (3.38 μM) over CARM1 (21.5 μM), PRMT5 (35.4 μM), and PRMT8 (84.9 μM), respectively.

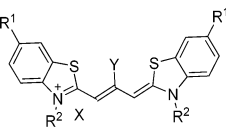
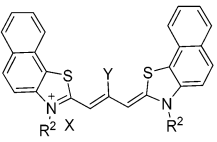
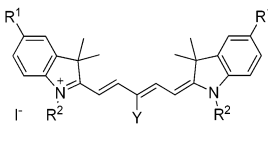
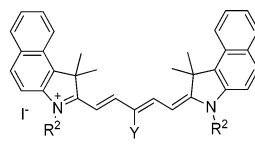
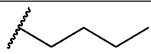
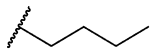
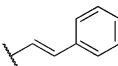
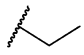
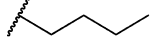
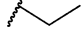
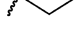
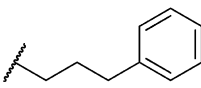
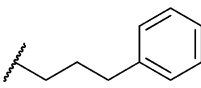
It is worthy to note that all the compounds but **50** showed steep slopes for the concentration–potency curves, with Hill coefficients (*n_H*) apparently higher than 1 (Figure 2, Table S2, Figure S1). There could be several explanations for it.⁵⁷ The first one could be that the compounds interacted with PRMT1 dimer or oligomer⁵⁸ in a positive cooperative way,⁵⁹ which means the binding of one ligand could enhance the affinity of the nearby site for the second ligand such that the IC₅₀ curve became steeper (so *n_H* larger than 1). The second possibility is that compound aggregates are the active form interacting with enzymes. This is possible considering the inhibition via aggregation is common in the early stage of drug discovery^{60,61} and cyanine dyes have a tendency to aggregate as π -stacked structures.⁵¹ This behavior is undesirable because it usually causes nonspecific binding and thus low selectivity. The third reason is that the compounds are tight binding inhibitors, which makes *K_d* much lower than the enzyme concentration. In this case, the IC₅₀ only relates to the enzyme concentration

other than reflecting the true *K_i*.^{57,59,62} Overall, there was a general observation that the compounds with high *n_H* exhibited a poor degree of selectivity. Compound **50**, on the other hand, has *n_H* approximate to unity for all the PRMTs, meaning it is most likely that this compound exerted inhibition through specific ligand–enzyme binding rather than by promiscuous interaction.

4. Compound 50 Binding with PRMT1. Because some PRMT inhibitors, such as NS-1 and TBBD (ellagic acid), act by binding with the substrate peptide instead of the enzyme, we also tried to detect the binding preference of compound **50**.^{43,63} We harnessed the fluorescence property of compound **50** and found its fluorescence intensity increased about 6-fold upon binding to PRMT1 (Figure S3). The binding affinity is 2.3 μM, which is in the close range of IC₅₀ value for PRMT1 inhibition. This validates that there is a direct interaction between compound **50** and PRMT1.

5. Docking. To better understand the obtained SAR, it is intriguing to investigate the interaction at the molecular level. Therefore, molecular simulations were used to begin speculating about the molecular recognition between **50** and PRMT1. The reported crystal structures (PDB codes 1ORI, 1OR8, and 1ORH) by Zhang and Cheng⁵⁸ provided substantial information on cofactor and substrate binding sites of rat

Table 3. Inhibition and IC₅₀ for Compounds with Modified Spacers

									
Cmpd# ^a	Name	R1	R2	Y	Inhibition (10 μM)	IC ₅₀ (sd) ^b	n _H (sd)		
40	AH-33	H		Me	77%				
41	EAO-50	H			48%				
48	AH-35			Me	92%	2.37 (0.116)	3.40 (0.50)		
50	E-84	Br		Br	96%	3.38 (0.14)	1.33 (0.09)		
51	MHI-86			H	89%	3.39 (0.144)	3.15 (0.41)		
52	MHI-114			Cl	69%				
53	E-16			H	70.20%	5.76 (0.46)	1.59 (0.19)		
54	E-38			Cl	96.30%	1.81 (0.10)	2.05 (0.20)		

^aCmpd# = compound number. ^bsd = standard deviation.

PRMT1 (rPRMT1). Nevertheless, the crystals were obtained at nonphysiological condition (pH 4.7), so they were considered inappropriate for virtual screening study.^{32–34,40,41}

Recently, we built a homology-modeled human PRMT1 (named HM-hPRMT1) from which the interaction between an inhibitor DB75 and hPRMT1 was revealed.⁴¹ On the basis of the HM-hPRMT1 structure, we attempted to perform a molecular docking on **50** using the implemented docking tool, CDORKER, of Discovery Studio.⁶⁴ Unfortunately, this initial trial failed. In the rPRMT1 crystal structure, the first 1–40 residues at N-terminal, including a conserved helix α X that contributes the recognition of SAM among PRMTs, were not resolved because of the disordered structure, indicating there was high flexibility of this sequence. In addition, several independent studies on the crystal structures of rat PRMT3,⁶⁵ mouse CARM1,^{66,67} and *Trypanosoma brucei* PRMT6⁶⁸ demonstrated the corresponding segments also had conformation alteration upon the binding of cofactor (SAM and SAH). On the basis of these facts, we postulated that the N-terminal acted as a “lid” of the pocket and could be adjusted to house ligands of different sizes. The failure of our first trial was probably because modeled SAM binding sites were too small to accommodate compound **50**. Therefore, we attempted to take the “lid” off the pocket by deleting the residues 1–40 in the HM-hPRMT1 (the resulting structure named PRMT1_ α X(–)) to get an enlarged binding pocket.

In the following docking study, a spherical area that covered both SAM and arginine binding pockets was chosen as the binding site (Figure S2) and the conformers ranking top 10 for the -CDOCKER_ENERGY values were generated. It turned out that there was no significant difference for these 10 conformers regarding the orientations (Figure 3C; the pocket surface was rendered according to hydrophobicity), which suggested **50** could fit the pocket very well. Conformer 1 (with the highest -CDOCKER_ENERGY value) was selected and superimposed with SAH (Figure 3A), which was maintained at the same orientation as in the crystal structure (PDB code 1OR8). As shown in Figure 3A, the binding site can be divided into three parts: a deeply buried pocket (BP), an exterior surface cavity (ESC), and a narrow channel connecting the two areas. The molecule of **50** spanned BP and ESC: (1) half of the molecule occupied the BP which comprised the site housing the adenosyl group of SAH and entrance of substrate arginine to the pocket; (2) the other half protruded out to the ESC area; (3) the pentamethine spacer bound to the channel. An analysis of the volume and hydrophobicity distribution of the pocket shed light on the underlying molecular basis for the summarized SAR: (1) Both the BP and ESC showed medium to high hydrophobicity with the highest areas located near the two distal bromines of compound **50**. This was consistent with the experimental phenomenon that higher hydrophobicity of

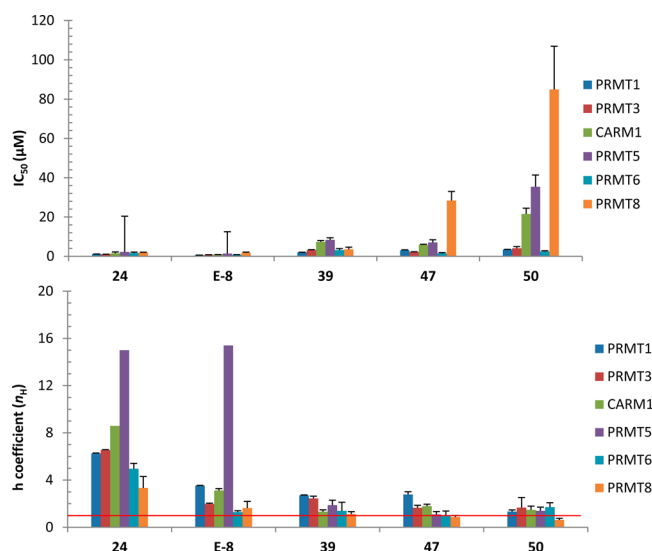


Figure 2. IC_{50} and n_H of compounds **24**, **E-8**, **39**, **47**, and **50** against PRMTs. Note that only compound **50** (**E-84**) shows satisfactory selectivity for PRMT1 as well as Hill coefficient around 1 against all PRMTs.

“heads” and “tails” resulted in better activities. (2) The BP seemed to fit one of the “head–tail” units of the compound very well, meaning the ligand can be fully contacted with this part. In contrast, the interaction between the molecule and ESC is much looser because of the larger volume of ESC, indicating the compound substituent in ESC can be replaced with a larger group to result in better spatial complementation in a future study. (3) The channel bridging BP and ESC was so narrow that even the bromine on spacer shifted slightly toward the BP to avoid the collision with pocket wall. This explained the poor activity of compound **41** in which there is a very bulky styryl group attached to the spacer.

A detailed inspection on the ligand–enzyme interaction revealed some hydrophobic, charge–charge, and hydrogen bond forces between the skeleton of **50** and side chains of surrounding residues (Figure 3B). The cation is delocalized across the nitrogen atoms of **50** at physiological pH and can involve electrostatic interactions and/or hydrogen bond, indicating their essential role in lowering the binding energy (thus increasing the binding affinity). Because a molecule may bind with protein with more than one orientation, it is more necessary to identify which residues make universal interactions with these poses and thus are essential for the ligand binding. Hence, the first 10 generated conformers of compound **50** were analyzed globally (Figure 3D). As for the residues, C101, E129, and M155 formed noncovalent bonds with all 10 conformers and K127 and E153 with no less than eight conformers. It is noteworthy that C101, E129, M155 are conserved residues among PRMT family that contribute to the SAM binding⁵⁸ and E153 was considered as a very essential residue for positioning the substrate arginine in a proper orientation to approach the methyl group (S^+Me) in SAM.^{58,69} The docking study suggested that the binding of compound **50** inhibited the activity of PRMT1 by impeding the correct positioning of both cofactor and substrate.

Nonetheless, it should be kept in mind that the above conclusion is just deduced on the basis of the docking results and we could not exclude the possibility that the compound can occupy the substrate peptide binding site. Actually, there are

several negatively charged grooves on the surface of PRMT1.⁵⁸ These grooves on the PRMT1 surface were considered as potential docking sites for the positively charged substrate segments, which usually are glycine- and arginine-rich (GAR) sequences.^{70,71} Though currently there is still no direct evidence that shows the small molecule inhibitors act by occupying peptide binding pocket for PRMTs, the situation is encouraging in the area of discovery of protein lysine transferases (PKMTs) inhibitors: AZ-505⁷² and BIX-01294⁷³ related compounds (e.g., UNC0224,⁷³ UNC0638,⁷⁴ and E72⁷⁵) have all been shown to interact with the peptide binding groove according to crystal structures, and the backbone amino groups in these molecules are involved in electrostatic or hydrogen-bond interaction. From this point of view, the positively charged cyanine compounds might also act by targeting the peptide binding groove on PRMT1.

6. Cellular Activity. In one of our previous reports,⁴¹ we showed that DB75, another PRMT1-specific inhibitor, has cell membrane permeable capability and blocks proliferation of leukemia cells. In order to determine whether compound **50** is also an intracellular PRMT1 inhibitor, we applied different concentrations of **50** to several leukemia cell cultures and then measured cellular proliferation by viability assays. We found that **50** was a powerful agent that significantly inhibited leukemia cell growth at 100 nM in Meg01 and MOLM13 cells and 200 nM in HEL cells (Figure 4A–C). HEL cells are more resistant to **E-84** than Meg01 and MOLM13 cells (Figure 4F) possibly because of HEL cells’ genetic background: the constitutively active JAK2 mutation makes cells less dependent on PRMT1-mediated signaling pathways. These results were consistent with what we have observed previously with DB75. At both 24 and 48 h of incubation, **50** showed a nanomolar level requirement for 50% inhibition (Figure 4F), indicating **50** can more efficiently target PRMT1 in cells than that of DB75. Cell pellets harvested from **50** supplemented culture showed a blue color (unpublished data), meaning **50** can permeate cell membrane and can be used as an intracellular PRMT1 stain. Treatment with **50** on leukemia cells led to significant loss of total protein arginine methylation (Figure 4G), demonstrating that **50** inhibited intracellular PRMT1 activity. All data above indicated that **50** permeated the cell membrane, inhibited intracellular PRMT1 activity, and blocked leukemia cell proliferation.

CONCLUSION

We reported herein a set of cyanine compounds as PRMT inhibitors. Among them, a pentamethine compound **E-84** (compound **50**) showed inhibition on PRMT1 with the potency at low micromolar level as well as specificity for PRMT1 over CARM1, PRMT5, and PRMT8 ranging from 6- to 25-fold. The following cellular activity studies showed that **E-84** permeated cell plasma membrane, decreased intracellular arginine methylation, and blocked leukemia cell proliferation. Besides, the structure–activity relationship for the cyanine compounds was systematically investigated with these features: (1) the two nitrogen-containing “head” is necessary for maintaining the activity; (2) increasing hydrophobicity generally leads to better inhibition; (3) a sulfur atom in position 3 of indolium group results in equal or better activity than dimethylmethine; (4) pentamethine as the spacer seems better than trimethine; (5) no larger than bromine can be tolerated on the *meso*-carbon of the spacer. Molecular docking study suggested **E-84** might act by partially occupying the cofactor

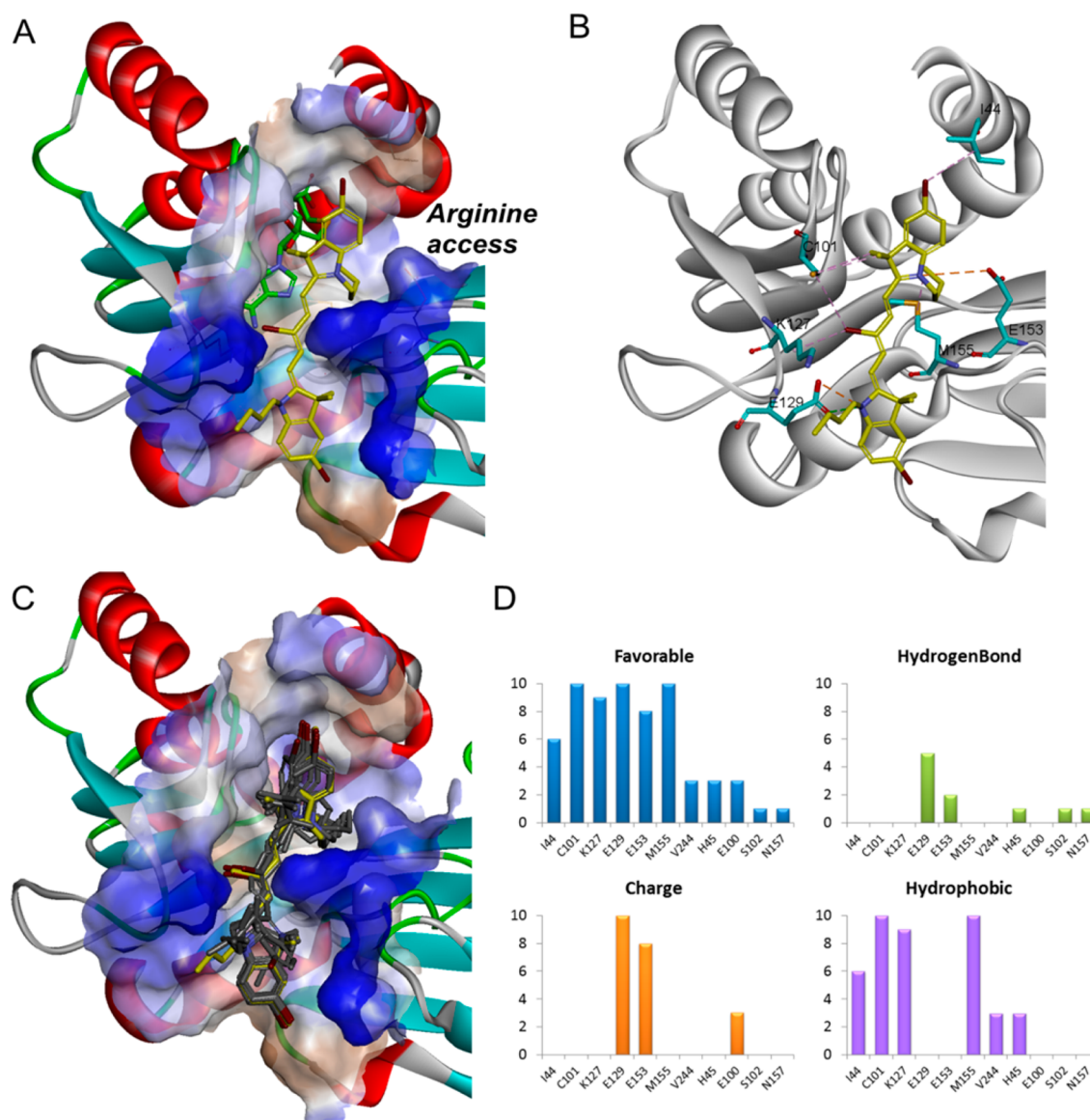


Figure 3. Docking result of compound **50**. (A) Binding pocket for compound **50**. The hydrophobic surface is rendered as brown and hydrophilic surface as blue. Conformer 1 of **50** (yellow) and SAH (green, retaining the same orientation as in crystal structure 1OR8) are shown in stick mode. The backbone of PRMT1_αX(-) is shown as ribbon. (B) Noncovalent bond interactions between the conformer 1 and residues. Conformer 1 (yellow) and the involved residues (cyanine) are shown in stick mode. Dash lines represent the interactions: hydrophobic interaction is colored as light purple, electrostatic force as brown, and hydrogen bond (H-bond) as green. (C) Overlapping of 10 conformers of **50** in the binding pocket with conformer 1 rendered as yellow and others as dark gray. Note there is no significant difference between the poses with regard to the spatial arrangement. (D) Histogram for the noncovalent bonds between 10 conformers and PRMT1_αX(-). Blue columns represent all the favorable interactions including hydrophobic interaction, electrostatic force, and H-bond. The colors of the columns in the other three histograms are the same as the corresponding interactions in (B).

binding site as well as blocking the proximity of cofactor and substrate arginine.

EXPERIMENTAL SECTION

1. Materials. The reagents for the synthesis of the final PRMT inhibiting agents were obtained commercially from Acros Organics or Matrix Scientific. Fmoc-protected amino acids and resins were purchased from NovaBioChem or ChemPep, and 2-(6-chloro-1H-benzotriazole-1-yl)-1,1,3,3-tetramethylaminium hexafluorophosphate (HCTU) was purchased from ChemPep. [³H]SAM (15 or 18 Ci/mmol). Streptavidin-coated PVT SPA beads were purchased from PerkinElmer. Isopropyl β-D-1-thiogalactopyranoside (IPTG) was obtained from RPI Corp. Other chemical reagents were purchased from Fisher, Sigma, and VWR. H3.3 protein was purchased from New England Biolabs.

2. Synthesis of Cyanine Compounds. All chemical reactions were maintained under a positive pressure of nitrogen unless otherwise stated. The reaction progress was monitored using silica gel 60 F₂₅₄ thin layer chromatography plates (Merck EMD Millipore, Darmstadt, Germany). Open column chromatography was utilized for the purification of all final compounds using 60–200 μm, 60A classic column silica gel (Dynamic Adsorbents, Norcross, GA). The nuclear magnetic resonance spectra were obtained using high quality Kontes NMR tubes (Kimble Chase, Vineland, NJ) rated to 500 MHz and were recorded on a Bruker Avance 400 MHz spectrometer interfaced to a PC using Topspin 3.1. High-resolution accurate mass spectra were obtained at the Georgia State University Mass Spectrometry Facility using a Waters Q-TOF micro (ESI-Q-TOF) mass spectrometer or utilizing a Waters Micromass LCT TOF ES+ Premier mass spectrometer. Liquid chromatography utilized a Waters 2487 single

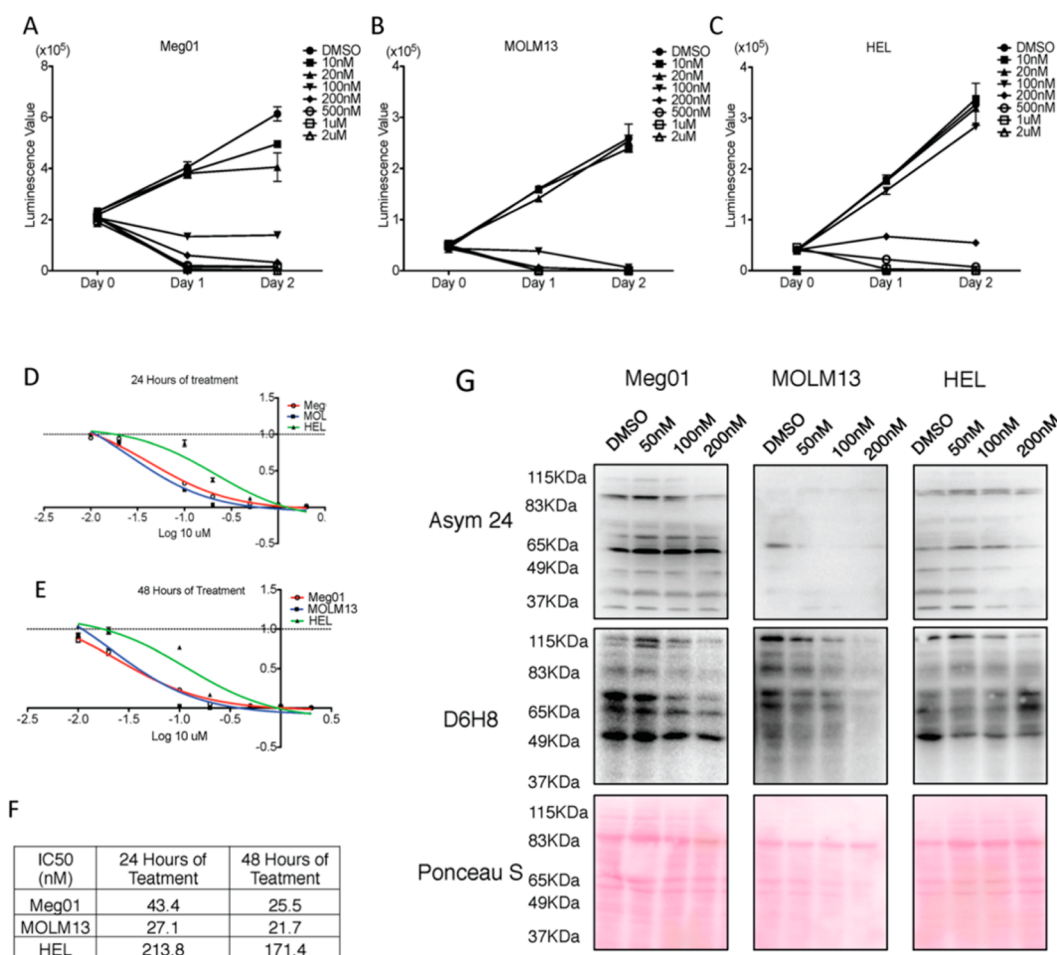


Figure 4. Compound **50** inhibited proliferation of leukemia cell lines via blocking of PRMT1 activity. (A–F) Compound **50** inhibited leukemic cell growth. Serial diluted **50** was added to the Meg01 (A), MOLM13 (B), and HEL (C) cell cultures, and each day the cell growth was measured by viability assay. As a control, the cells were treated with the same volume of DMSO as that added in 2 μ M **50** treated samples. (D) Drug sensitivity curves of all cell lines after 24 h of treatment of **50**. (E) Drug sensitivity curves of all cell lines after 48 h of treatment of **50**. (F) Calculated IC₅₀ concentration of **50** for all cell lines. (G) Arginine methylation level of **50**-treated leukemic cells. Meg01, MOLM13, and HEL cells were cultured with the presence of **50** or DMSO. Extract was harvested after 24 h of treatment, and samples were resolved by SDS–PAGE. Arginine methylation status was detected by using anti-methyl-R antibodies.

wavelength absorption detector with wavelengths set between 640 and 700 nm depending on the particular photophysical properties. The column used in LC was a Waters Delta-Pak 5 μ m, 100A 3.9 mm \times 150 mm reversed phase C₁₈ column. Evaporative light scattering detection analyzes trace impurities that cannot be observed by alternative methods; a SEDEX 75 ELSD was utilized in tandem with liquid chromatography to confirm purity. Integrals for the ELSD and absorption peaks were utilized to confirm >95% purity for all final compounds that were tested in PRMT inhibition assays.

The synthetic procedures for **1–9** and **17–21** have been previously reported by our laboratory and were utilized in the subsequent reactions without purification or modification.

Synthesis of Halogenated Trimethine Cyanines with Indolenine Heterocycle (22–27). Appropriate heterocyclic salt was added to an oven dried round-bottom flask which was filled with nitrogen. Acetic anhydride (5 mL) was added to the round-bottom flask, and the solution was heated to 90 $^{\circ}$ C. Triethyl orthoformate (3 mol equiv) was added via syringe to the stirring solution. After 30 min, the reaction turned bright-pink and the reaction progress was monitored using UV–vis spectrophotometry and TLC, eluting with 5% methanol in DCM. After consumption of the starting materials, the reaction mixture was allowed to cool and the solution was triturated with ether, resulting in the precipitation of the product. The compounds were isolated using silica gel chromatography with gradient elution from 10% hexanes in DCM to 5% methanol in DCM. The

column fractions were combined and concentrated to afford the pure products.

5-Bromo-2-((E)-3-((E)-5-bromo-1-ethyl-3,3-dimethylindolin-2-ylidene)prop-1-en-1-yl)-1-ethyl-3,3-dimethyl-3H-indol-1-ium iodide (22). ¹H NMR (400 MHz, DMSO-*d*₆) δ 1.295 (d, *J* = 6.4 Hz, 6H), 1.696 (s, 12H), 4.153 (d, *J* = 6.4 Hz, 4H), 6.559 (d, *J* = 13.2 Hz, 2H), 7.515 (s, 4H), 7.835 (s, 2H), 8.316 (t, *J* = 13.2 Hz, 1H); ¹³C NMR (100 MHz, DMSO-*d*₆) δ 12.67, 27.64, 49.59, 103.39, 113.31, 123.58, 129.06, 130.10, 140.88, 143.28, 173.91. 67% yield; mp >260 $^{\circ}$ C.

1-Butyl-2-((E)-3-((E)-1-butyl-5-chloro-3,3-dimethylindolin-2-ylidene)prop-1-en-1-yl)-5-chloro-3,3-dimethyl-3H-indol-1-ium iodide (23). ¹H NMR (400 MHz, DMSO-*d*₆) δ 0.932 (t, *J* = 6.4 Hz, 6H), 1.410 (d, *J* = 6.8 Hz, 4H), 1.697 (s, 16H), 4.131 (s, 4H), 6.597 (d, *J* = 13.2 Hz, 2H), 7.505 (s, 4H), 7.827 (s, 2H), 8.321 (t, *J* = 13.2 Hz, 1H); ¹³C NMR (100 MHz, DMSO-*d*₆) δ 14.28, 19.98, 27.74, 29.64, 44.43, 49.58, 103.61, 113.59, 123.51, 129.03, 130.09, 141.32, 143.19, 150.52, 174.31. 54% yield; mp >260 $^{\circ}$ C.

5-Chloro-2-((E)-3-((E)-5-chloro-3,3-dimethyl-1-(3-phenylpropyl)-indolin-2-ylidene)prop-1-en-1-yl)-3,3-dimethyl-1-(3-phenylpropyl)-3H-indol-1-ium Bromide (24). ¹H NMR (400 MHz, DMSO-*d*₆) δ 1.681 (s, 12H), 2.036 (s, 4H), 2.766 (s, 4H), 4.179 (s, 4H), 6.424 (d, *J* = 12.4 Hz, 2H), 7.204 (m, 10H), 7.466 (d, *J* = 8.0 Hz, 4H), 7.818 (s, 2H), 8.293 (t, *J* = 13.2 Hz, 1H); ¹³C NMR (100 MHz, DMSO-*d*₆) δ 27.70, 29.15, 32.52, 44.31, 49.62, 103.54, 113.49, 123.52, 126.54,

128.72, 128.86, 129.02, 130.14, 141.29, 141.36, 143.20, 150.42, 174.35; 59% yield; mp >260 °C.

5-Bromo-2-((E)-3-((E)-5-bromo-1-ethyl-3,3-dimethylindolin-2-ylidene)prop-1-en-1-yl)-1-ethyl-3,3-dimethyl-3H-indol-1-ium Iodide (25). ¹H NMR (400 MHz, DMSO-*d*₆) δ 1.308 (t, *J* = 7.2 Hz, 6H), 1.693 (s, 12H), 4.148 (m, *J* = 7.2 Hz, 4H), 6.565 (d, *J* = 13.2 Hz, 2H), 7.446 (d, *J* = 8.4 Hz, 2H), 7.634 (d, *J* = 8.4 Hz, 2H), 7.948 (s, 2H), 8.316 (t, *J* = 13.2 Hz, 1H); ¹³C NMR (100 MHz, DMSO-*d*₆) δ 12.67, 27.64, 49.58, 103.42, 113.75, 118.11, 126.32, 131.91, 141.30, 143.58, 150.59, 173.76; 65% yield; mp >260 °C.

5-Bromo-2-((E)-3-((E)-5-bromo-1-butyl-3,3-dimethylindolin-2-ylidene)prop-1-en-1-yl)-1-butyl-3,3-dimethyl-3H-indol-1-ium Iodide (26). ¹H NMR (400 MHz, DMSO-*d*₆) δ 0.934 (t, *J* = 7.2 Hz, 6H), 1.410 (q, *J* = 7.2 Hz, 4H), 1.696 (s, 16H), 4.121 (t, *J* = 7.2 Hz, 4H), 6.570 (d, *J* = 13.6 Hz, 2H), 7.455 (d, *J* = 8.4 Hz, 2H), 7.635 (d, *J* = 8.4 Hz, 2H), 7.945 (s, 2H), 8.320 (t, *J* = 13.2 Hz, 2H); ¹³C NMR (100 MHz, DMSO-*d*₆) δ 14.28, 19.98, 27.74, 29.62, 44.41, 49.59, 103.61, 114.02, 118.13, 126.26, 131.88, 141.75, 143.49, 174.19; 73% yield, mp 265–268 °C.

5-Bromo-2-((E)-3-((E)-5-bromo-3,3-dimethyl-1-(3-phenylpropyl)-indolin-2-ylidene)prop-1-en-1-yl)-3-dimethyl-1-(3-phenylpropyl)-3H-indol-1-ium Bromide (27). ¹H NMR (400 MHz, DMSO-*d*₆) δ 1.694 (s, 12H), 2.038 (q, *J* = 7.2 Hz, 4H), 2.772 (t, *J* = 8.0 Hz, 4H), 4.181 (t, *J* = 7.2 Hz, 4H), 6.442 (d, *J* = 13.6 Hz, 2H), 7.192 (d, *J* = 8.8 Hz, 4H), 7.243 (m, 6H), 7.399 (d, *J* = 8.4 Hz, 2H), 7.618 (d, *J* = 7.6 Hz, 2H), 7.939 (s, 2H), 8.302 (t, *J* = 13.2, 1H); ¹³C NMR (100 MHz, DMSO-*d*₆) δ 27.71, 29.16, 44.28, 49.61, 103.58, 113.93, 118.17, 126.26, 126.54, 126.59, 128.73, 128.86, 141.36, 141.71, 143.49, 174.20; 78% yield; mp >260 °C.

Compounds **28–33** were prepared according to literature procedure without modification and were used without purification in the proceeding steps.

Synthesis of Benzothiazole Trimethine Cyanines 34–39. Benzothiazole heterocyclic salt (1 mol equiv) bearing alkyl groups on the heterocyclic nitrogen was added to a round-bottom flask followed by acetic anhydride (5 mL). This mixture was heated to 90 °C, and triethyl orthoformate (3 mol equiv) was added to the reaction mixture. After 15 min, the reaction solution turned deep purple indicating the progress on the reaction. After the reaction was completed as indicated by TLC analyses, the contents were allowed to cool and diethyl ether was added. The flask was cooled on an ice bath for 1 h, and crystals began to develop. These crystals were filtered and washed with ether and hexanes. The pure compounds were isolated using column chromatography.

3-Ethyl-2-((1E,3Z)-3-(3-ethylbenzo[d]thiazol-2(3H)-ylidene)prop-1-en-1-yl)benzo[d]thiazol-3-ium Iodide (34). ¹H NMR (400 MHz, DMSO-*d*₆) δ 1.35 (t, *J* = 6.8 Hz, 6H), 4.39 (d, *J* = 6.8 Hz, 4H), 6.63 (d, *J* = 13.2 Hz, 2H), 7.43 (t, *J* = 7.6 Hz, 2H), 7.58 (t, *J* = 8.0 Hz, 2H), 7.80 (m, 3H), 8.01 (d, *J* = 7.6 Hz, 2H); ¹³C NMR (100 MHz, DMSO-*d*₆) δ 13.08, 21.53, 41.94, 99.10, 113.84, 123.59, 125.67, 128.59, 141.27, 147.13, 164.64; 72% yield; mp >260 °C.

3-Butyl-2-((1E,3Z)-3-(3-butylbenzo[d]thiazol-2(3H)-ylidene)prop-1-en-1-yl)benzo[d]thiazol-3-ium Iodide (35). ¹H NMR (400 MHz, DMSO-*d*₆) δ 0.94 (t, *J* = 7.2 Hz, 6H), 1.43 (m, 4H), 1.72 (m, 4H), 4.34 (t, *J* = 7.2 Hz, 4H), 6.62 (d, *J* = 12.8 Hz, 2H), 7.43 (t, *J* = 7.6 Hz, 2H), 7.58 (t, *J* = 7.6 Hz, 2H), 7.78 (m, 3H), 8.00 (d, *J* = 7.6 Hz, 2H); ¹³C NMR (100 MHz, DMSO-*d*₆) δ 13.70, 19.41, 29.44, 46.08, 98.78, 113.64, 123.06, 125.22, 128.08, 139.48, 141.26, 146.68, 164.62; 66% yield; mp >260 °C.

3-(3-Phenylpropyl)-2-((1E,3Z)-3-(3-(3-phenylpropyl)benzo[d]thiazol-2(3H)-ylidene)prop-1-en-1-yl)benzo[d]thiazol-3-ium Bromide (36). ¹H NMR (400 MHz, DMSO-*d*₆) δ 2.09 (t, *J* = 7.2 Hz, 4H), 2.79 (m, 4H), 4.38 (t, *J* = 7.2 Hz, 4H), 6.43 (d, *J* = 12.0 Hz, 2H), 7.26 (m, 12H), 7.56 (t, *J* = 6.8 Hz, 2H), 7.69 (d, *J* = 7.2 Hz, 2H), 7.76 (t, *J* = 12.8 Hz, 1H), 7.99 (d, *J* = 7.2 Hz, 2H); ¹³C NMR (100 MHz, DMSO-*d*₆) δ 28.57, 31.78, 45.82, 113.37, 122.89, 125.09, 125.94, 127.91, 128.05, 128.25, 140.51, 141.07; HRMS calcd for C₃₃H₃₃N₂S₂⁺ *m/z* 545.2080, obsd *m/z* 545.2061; 67% yield; mp 220–221 °C.

6-Bromo-2-((1E,3Z)-3-(6-bromo-3-ethylbenzo[d]thiazol-2(3H)-ylidene)prop-1-en-1-yl)-3-ethylbenzo[d]thiazol-3-ium Iodide (37). ¹H NMR (400 MHz, DMSO-*d*₆) δ 1.32 (t, *J* = 6.8 Hz, 6H), 4.36

(q, *J* = 6.8 Hz, 4H), 6.62 (d, *J* = 12.4 Hz, 2H), 7.74 (m, 4H), 7.82 (t, *J* = 12.8 Hz, 1H), 8.29 (s, 2H); ¹³C NMR (100 MHz, DMSO-*d*₆) δ 13.01, 42.20, 115.48, 117.61, 125.97, 127.93, 131.38; 46% yield.

6-Bromo-2-((1E,3Z)-3-(6-bromo-3-butylbenzo[d]thiazol-2(3H)-ylidene)prop-1-en-1-yl)-3-butylbenzo[d]thiazol-3-ium Iodide (38). ¹H NMR (400 MHz, DMSO-*d*₆) δ 0.93 (t, *J* = 7.2 Hz, 6H), 1.42 (m, 4H), 1.69 (m, 4H), 4.31 (t, *J* = 7.2 Hz, 4H), 6.62 (d, *J* = 12.8 Hz, 2H), 7.77 (m, 5H), 8.28 (s, 2H); ¹³C NMR (100 MHz, DMSO-*d*₆) δ 14.15, 19.83, 29.85, 46.80, 99.84, 115.73, 117.63, 125.91, 127.77, 131.34, 141.20, 147.52, 165.24; HRMS calcd for C₂₅H₂₇Br₂N₂S₂⁺ *m/z* 576.9977, obsd *m/z* 576.9983; 76% yield; mp >260 °C.

5-Bromo-2-((1E,3Z)-3-(5-bromo-3-butylbenzo[d]thiazol-2(3H)-ylidene)prop-1-en-1-yl)-3-butylbenzo[d]thiazol-3-ium Iodide (39). ¹H NMR (400 MHz, DMSO-*d*₆) δ 0.94 (t, *J* = 7.2 Hz, 6H), 1.45 (m, 4H), 1.68 (m, 4H), 4.33 (t, *J* = 7.2 Hz, 4H), 6.63 (d, *J* = 12.8 Hz, 2H), 7.60 (d, *J* = 8.4 Hz, 2H), 7.79 (t, *J* = 12.8 Hz, 1H), 7.95 (d, *J* = 8.4 Hz, 2H), 8.08 (s, 2H); ¹³C NMR (100 MHz, DMSO-*d*₆) δ 0.58, 14.20, 19.78, 29.91, 46.70, 100.02, 116.78, 121.59, 125.06, 125.10, 128.43, 143.14, 147.65; HRMS calcd for C₂₅H₂₇Br₂N₂S₂⁺ *m/z* 576.9977, obsd *m/z* 576.9983; 77% yield; mp >260 °C.

Synthesis of Benzothiazole cyanine with meso-Methyl Moiety 40. Butylated benzothiazole salt (1 mol equiv) was added to a round-bottom flask, and triethyl orthoacetate (10 mol equiv) was added followed by freshly distilled pyridine (7 mL). The resulting mixture was refluxed under heavy stirring for 4 h. The bright pink solution was allowed to cool. Ether (100 mL) was added to the round-bottom flask, and it was allowed to stand for 2 h. The resulting pink crystals were filtered and dissolved in DCM. The pink solution was washed with water, sat. solution of sodium bicarbonate, and brine. The organic layer was combined and concentrated to afford the meso-methylated benzothiazole carbocyanine PRMT binding agent **40**.

3-Butyl-2-((1E,3Z)-3-(3-butylbenzo[d]thiazol-2(3H)-ylidene)-2-methylprop-1-en-1-yl)benzo[d]thiazol-3-ium Iodide (40). ¹H NMR (400 MHz, MeOD-*d*₄) δ 1.080 (t, *J* = 7.2 Hz, 6H), 1.607 (m, 4H), 1.934 (p, *J* = 7.2 Hz, 4H), 2.698 (s, 3H), 4.495 (t, *J* = 7.2 Hz, 4H), 6.553 (s, 2H), 7.463 (t, *J* = 7.6 Hz, 2H), 7.650 (t, *J* = 7.6 Hz, 2H), 7.730 (d, *J* = 8.4 Hz, 2H), 7.926 (d, *J* = 8.0 Hz, 2H); ¹³C NMR (100 MHz, DMSO-*d*₆) δ 14.24, 19.93, 29.60, 46.67, 14.05, 123.38, 123.44, 125.32, 125.86, 128.79, 128.85, 140.41, 160.49; 74% yield; mp >260 °C.

Synthesis of Styryl-Modified Cyanine 41. Precursor **40** (1 mol equiv) was added to a round-bottom flask followed by benzaldehyde (12 mol equiv) followed by ethanol (5 mL) and piperidine (5 mol equiv). The resulting mixture was heated to reflux for 12 h and was followed by a shift in the absorption spectrum and TLC. The pink colored starting solution gradually turned deep purple resulting in the formation of the product. After the starting material was consumed, the reaction mixture was concentrated and extracted in DCM. The organic layer was washed with sat. sodium bicarbonate and brine, dried over sodium sulfate, and concentrated. The residue was purified with open column chromatography, eluting with 3% methanol in DCM to obtain the pure compound with a meso-styryl group.

3-Butyl-2-((1E,3E)-2-((Z)-3-butylbenzo[d]thiazol-2(3H)-ylidene)-methyl)-4-phenylbuta-1,3-dien-1-yl)benzo[d]thiazol-3-ium Iodide (41). ¹H NMR (400 MHz, CDCl₃) δ 1.013 (s, 6H), 1.260 (s, 4H), 1.660 (s, 4H), 1.933 (s, 4H), 4.631 (s, 4H), 6.983 (s, 2H), 7.696–7.258 (m, 15H); ¹³C NMR (100 MHz, DMSO-*d*₆) δ 14.15, 19.90, 29.96, 46.73, 110.22, 113.82, 123.25, 125.43, 126.40, 128.45, 128.69, 129.58, 130.15, 136.32, 140.63, 140.70, 161.82.

3-Ethyl-2-methylnaphtho[2,1-d]thiazol-3-ium Iodide (42). ¹H NMR (400 MHz, DMSO-*d*₆) δ 1.51 (t, *J* = 7.2 Hz, 3H), 3.30 (s, 3H), 4.88 (q, *J* = 7.2 Hz, 2H), 7.87 (m, 2H), 8.30 (d, *J* = 8.0 Hz, 1H), 8.43 (m, 3H); 75% yield.

3-Butyl-2-methylnaphtho[2,1-d]thiazol-3-ium Iodide (43). ¹H NMR (400 MHz, DMSO-*d*₆) δ 0.95 (t, *J* = 7.2 Hz, 3H), 1.49 (q, *J* = 7.2 Hz, 2H), 1.884 (m, 2H), 3.31 (s, 3H), 4.83 (t, *J* = 7.2 Hz, 1H), 7.86 (m, 2H), 8.30 (d, *J* = 7.6 Hz, 1 H), 8.41 (m, 3H); 90% yield.

2-Methyl-3-(3-phenylpropyl)naphtho[2,1-d]thiazol-3-ium Bromide (44). Compound **44** was used without purification.

Synthesis of Napthathiazole-Based Trimethine Cyanines. Corresponding alkylated heterocycle was added to an oven-dried and

nitrogen cooled round-bottom flask followed by acetic anhydride (8 mL) and triethyl orthoformate (3 mol equiv). The reaction mixture was heated at 90 °C, and the reaction was monitored using UV-vis and TLC. After the starting materials were consumed, the reaction mixture was poured into diethyl ether under heavy stirring resulting in the precipitation of the compound. The crystals were filtered and isolated using column chromatography to obtain the final binding agents.

3-Ethyl-2-((1E,3Z)-3-(3-ethylnaphtho[2,1-d]thiazol-2(3H)-ylidene)prop-1-en-1-yl)naphtho[2,1-d]thiazol-3-ium iodide (45). ¹H NMR (400 MHz, DMSO-*d*₆) δ 1.40 (t, *J* = 6.4 Hz, 6H), 4.47 (q, *J* = 6.0 Hz, 4H), 6.67 (d, *J* = 12.4 Hz, 2H), 7.55 (t, *J* = 7.6 Hz, 2H), 7.93 (m, 5H), 8.06 (d, *J* = 7.2 Hz, 2H), 8.14 (d, *J* = 7.6 Hz, 2H); ¹³C NMR (100 MHz, DMSO-*d*₆) δ 13.47, 42.43, 99.21, 113.18, 121.40, 123.52, 126.75, 127.00, 129.07, 129.59, 129.93, 130.64, 139.39, 145.86, 163.44; HRMS calcd for C₂₉H₂₅N₂S₂⁺ *m/z* 465.1454, obsd *m/z* 465.1455; 70% yield; mp >260 °C.

3-Butyl-2-((1E,3Z)-3-(3-butylnaphtho[2,1-d]thiazol-2(3H)-ylidene)prop-1-en-1-yl)naphtho[2,1-d]thiazol-3-ium iodide (46). ¹H NMR (400 MHz, DMSO-*d*₆) δ 0.96 (t, *J* = 7.2 Hz, 6H), 1.47 (m, 4H), 1.78 (m, 4H), 4.45 (t, *J* = 7.2 Hz, 4H), 6.69 (d, *J* = 12.8 Hz, 2H), 7.61 (t, *J* = 8.0 Hz, 2H), 7.74 (t, *J* = 8.0 Hz, 2H), 7.93 (m, 5H), 8.10 (d, *J* = 8.0 Hz, 2H), 8.16 (d, *J* = 9.2 Hz, 2H); ¹³C NMR (100 MHz, DMSO-*d*₆) δ 14.22, 19.88, 30.28, 47.00, 99.44, 113.48, 121.30, 123.59, 126.71, 127.11, 129.15, 129.65, 129.88, 130.65, 139.86, 145.96, 163.86; HRMS calcd for C₃₃H₃₃N₂S₂⁺ *m/z* 521.2080, obsd *m/z* 521.2075; 60% yield; mp >260 °C.

3-(3-Phenylpropyl)-2-((1E,3Z)-3-(3-(3-phenylpropyl)naphtho[2,1-d]thiazol-2(3H)-ylidene)prop-1-en-1-yl)naphtho[2,1-d]thiazol-3-ium iodide (47). ¹H NMR (400 MHz, DMSO-*d*₆) δ 2.15 (m, 4H), 2.82 (m, 4H), 4.515 (m, 4H), 6.52 (d, *J* = 12.4 Hz, 2H), 7.21 (m, 2H), 7.28 (m, 7H), 7.64 (t, *J* = 7.6 Hz, 2H), 7.76 (t, *J* = 7.6 Hz, 2H), 7.92 (m, 3H), 8.00 (d, *J* = 8.0 Hz, 2H), 8.15 (t, *J* = 9.6 Hz, 4H); ¹³C NMR (100 MHz, DMSO-*d*₆) δ 29.60, 32.34, 46.82, 113.39, 121.42, 123.60, 126.59, 126.74, 127.16, 128.70, 128.90, 129.19, 129.69, 129.88, 130.69, 139.86, 141.18, 145.94; HRMS calcd for C₄₃H₃₇N₂S₂⁺ *m/z* 645.2393, obsd *m/z* 645.2375; 50% yield; mp 231–233 °C.

Synthesis of meso-Methylated Naphthothiazole Compound 48. 3-Ethyl-2-((1E,3Z)-3-(3-ethylnaphtho[2,1-d]thiazol-2(3H)-ylidene)-2-methylprop-1-en-1-yl)naphtho[2,1-d]thiazol-3-ium iodide (48). ¹H NMR (400 MHz, DMSO-*d*₆) δ 1.51 (t, *J* = 6.8 Hz, 6H), 2.74 (s, 3H), 4.67 (q, *J* = 6.8 Hz, 4H), 6.72 (m, 2H), 7.66 (t, *J* = 7.6 Hz, 2H), 7.78 (t, *J* = 7.6 Hz, 2H), 8.07 (m, 2H), 8.11 (d, *J* = 8.4 Hz, 2H), 8.16 (d, *J* = 8.0 Hz, 2H), 8.23 (d, *J* = 9.2 Hz, 2H).

Pentamethine precursor 49 has been previously described by our lab and was used as described without any additional modifications or purification.⁵⁶

Synthesis of Pentamethine Cyanine Binding Agents 50–54. Corresponding heterocyclic derivative (1 mol equiv) was added to a round-bottom flask followed by the pentamethine precursor (2 mol equiv). This mixture was dissolved in acetic anhydride (5 mL), and sodium acetate was added (4 mol equiv). The solution was stirred and heated to 60 °C for 2–4 h or until TLC indicated the complete reaction of starting materials. The reaction mixture was allowed to cool, and diethyl ether was added to the round-bottom flask. The obtained crystals were dissolved in DCM and gravity-filtered to remove unreacted sodium acetate from the final compound. The liquid was concentrated and purified on column chromatography, eluting with 2–5% methanol in DCM.

5-Bromo-2-((1E,3Z)-3-bromo-5-((E)-5-bromo-1-butyl-3,3-dimethylindolin-2-ylidene)penta-1,3-dien-1-yl)-1-butyl-3,3-dimethyl-3H-indol-1-ium iodide (50). ¹H NMR (400 MHz, DMSO-*d*₆) δ 0.936 (t, *J* = 7.2 Hz, 6H), 1.377 (q, *J* = 7.2 Hz, 4H), 1.727 (s, 16H), 4.178 (bs, 4H), 6.340 (d, *J* = 13.2 Hz, 2H), 7.498 (d, *J* = 8.4 Hz, 2H), 7.630 (d, *J* = 8.4 Hz, 2H), 8.031 (s, 2H), 8.466 (d, *J* = 13.2 Hz, 2H); ¹³C NMR (100 MHz, DMSO-*d*₆) δ 14.12, 19.93, 26.96, 29.38, 44.31, 50.10, 100.67, 114.20, 118.52, 123.23, 126.44, 131.76, 141.63, 144.25, 148.19, 174.47; 61% yield; mp 260–262 °C.

3-Ethyl-2-((1E,3E,5E)-5-(3-ethyl-1,1-dimethyl-1H-benzo[e]indol-2(3H)-ylidene)penta-1,3-dien-1-yl)-1,1-dimethyl-1H-benzo[e]indol-3-ium iodide (51). ¹H NMR (400 MHz, DMSO-*d*₆) δ 1.333 (t, *J* = 8

Hz, 6H), 1.962 (s, 12H), 4.297 (t, *J* = 8 Hz, 4H), 6.37 (d, *J* = 12 Hz, 2H), 6.637 (t, *J* = 12 Hz, 1H), 7.51 (t, *J* = 8 Hz, 2H), 6.68 (t, *J* = 8 Hz, 2H), 7.74 (d, *J* = 8 Hz, 2H), 8.08 (t, *J* = 8 Hz, 4H), 8.25 (d, *J* = 8 Hz, 2H), 8.46 (t, *J* = 12 Hz, 2H); ¹³C NMR (100 MHz, DMSO-*d*₆) δ 11.96, 26.17, 48.04, 50.19, 102.05, 110.90, 121.58, 124.20, 125.07, 127.11, 127.19, 129.39, 129.83, 130.76, 132.72, 138.77, 152.54, 172.71; HRMS calcd for [C₃₇H₃₉N₂]⁺ 511.3113, found 511.3098; 79% yield; mp 266–268 °C.

2-((1E,3Z,5E)-3-Chloro-5-(3-ethyl-1,1-dimethyl-1H-benzo[e]indol-2(3H)-ylidene)penta-1,3-dien-1-yl)-3-ethyl-1,1-dimethyl-1H-benzo[e]indol-3-ium iodide (52). ¹H NMR (400 MHz, DMSO-*d*₆) δ 1.39 (s, 6H), 2.00 (s, 12H), 4.37 (s, 4H), 6.38 (d, *J* = 16 Hz, 2H), 7.55 (t, 2H), 7.73 (t, 2H), 7.84 (d, *J* = 8 Hz, 2H), 8.12 (m, 4H), 8.27 (d, *J* = 4 Hz, 2H), 8.65 (d, *J* = 16 Hz, 2H); ¹³C NMR (100 MHz, DMSO-*d*₆) δ 11.81, 25.80, 50.72, 98.52, 111.19, 121.60, 121.71, 124.67, 126.96, 127.37, 129.47, 130.01, 131.15, 133.41, 138.56, 146.10, 174.17; HRMS calcd for [C₃₇H₃₈N₂Cl]⁺ 545.2724, found 545.2717; 68% yield; mp 231–233 °C.

2-((1E,3E,5E)-5-(1,1-Dimethyl-3-(3-phenylpropyl)-1H-benzo[e]indol-2(3H)-ylidene)penta-1,3-dien-1-yl)-1,1-dimethyl-3-(3-phenylpropyl)-1H-benzo[e]indol-3-ium iodide (53). ¹H NMR (400 MHz, DMSO-*d*₆) δ 1.95 (s, 12H), 2.05 (t, 8.4 Hz, 4H), 2.78 (t, *J* = 8.0 Hz, 4H), 4.29 (t, *J* = 6.8 Hz, 4H), 6.27 (d, *J* = 13.6 Hz, 2H), 6.55 (t, *J* = 12.4 Hz, 1H), 7.31–7.17 (m, 10H), 7.49 (t, *J* = 11.2 Hz, 2H), 7.72–7.64 (m, 4H), 8.07–8.03 (m, 4H), 8.24 (d, *J* = 8.4 Hz, 2H), 8.49 (t, *J* = 13.2 Hz, 2H); ¹³C NMR (100 MHz, DMSO-*d*₆) δ 27.24, 29.53, 32.55, 43.74, 51.19, 103.40, 112.01, 119.44, 122.59, 125.21, 125.54, 128.05, 128.19, 128.73, 128.90, 130.38, 130.75, 131.74, 133.63, 140.13, 141.49, 153.41, 174.13; HRMS calcd for [C₅₁H₅₁N₂]⁺ 691.4052, found 691.4028; 33% yield; mp 95–98 °C.

2-((1E,3Z,5E)-3-Chloro-5-(1,1-dimethyl-3-(3-phenylpropyl)-1H-benzo[e]indol-2(3H)-ylidene)penta-1,3-dien-1-yl)-1,1-dimethyl-3-(3-phenylpropyl)-1H-benzo[e]indol-3-ium Bromide (54). ¹H NMR (400 MHz, DMSO-*d*₆) δ 1.98 (s, 12H), 2.04 (t, *J* = 4.0 Hz, 4H), 2.82 (t, *J* = 4.0 Hz, 4H), 4.31 (t, *J* = 8.0 Hz, 4H), 6.235 (d, *J* = 16.0 Hz, 2H), 7.23–7.36 (m, 10H), 7.57 (t, *J* = 8.0 Hz, 2H), 7.72 (t, *J* = 8.0 Hz, 2H), 7.82 (d, *J* = 8.0 Hz, 2H), 8.12 (t, *J* = 8.0 Hz, 4H), 8.28 (d, *J* = 8.0 Hz, 2H), 8.58 (d, *J* = 12.0 Hz, 2H); ¹³C NMR (100 MHz, DMSO-*d*₆) δ 27.65, 29.77, 33.39, 44.93, 52.44, 100.59, 112.99, 123.47, 123.60, 126.49, 127.42, 128.68, 129.17, 129.55, 129.80, 131.22, 131.73, 132.90, 135.16, 140.62, 141.89, 147.75, 176.31; HRMS calcd for C₅₁H₅₀N₂Cl 725.3663, found 725.3663; 47% yield; mp 165–168 °C.

3. Peptide Synthesis. Peptides were synthesized using standard solid phase peptide synthesis protocols, purified on C-18 RP-HPLC, and confirmed with MALDI-MS as described before.^{43,76,77} The sequence of the NH₂-terminal 20 aa peptide of histone H4, H4(1–20), is Ac-SGRGKGGKGLGKGGAKRHRK. The sequence of K20-biotinated H4(1–20), H4(1–20)_{BTN}, is Ac-SGRGKGGKGLGKGGAKRHRK(biotin). The biotin is connected to the side chain amino group. The sequence of the glycine- and arginine-rich peptide, R4, is Ac-GGRGGFGGRGGKGGRRGGFGGRGGFG. Underlined R letters are the arginines that are methylated in the assay.

4. Protein Expression and Purification. PRMT1, -3, -6, and -8 are His6x-tagged proteins, and PRMT4 (usually also called CARM1) is a GST-tagged protein. The expression and purification have been described in previous work.^{41–43,48,77–79} Generally speaking, the plasmid was transformed into *E. coli* BL21(DE3) using heat shock method and the expression of protein was induced with IPTG. Next, bacteria were precipitated and harvested by centrifugation, followed by cell lysis in cell disruptor. Then His6x-tagged protein was purified on Ni-NTA beads and GST-tagged protein on glutathione agarose beads. Protein concentration was determined with Bradford assay.

5. Single-Dose Inhibition Study with PRMT1 Enzyme. Scintillation proximity assay (SPA)⁵² was performed in a 96-well plate at room temperature (about 25 °C). The reaction buffer contained 50 mM HEPES (pH 8.0), 1 mM EDTA, 50 mM NaCl, and 0.5 mM dithiothreitol (DTT). In the tested group, 6 μL of compound (10, 30, or 90 μM) was incubated with 18 μL mixture of [³H]-labeled SAM (0.5 μM) and His6x-PRMT1 (0.02 μM) for 5 min before initiating the reaction with the addition of 6 μL of H4(1–20)_{BTN}

peptide (1 μ M). After 8 min, the reaction was quenched with 30 μ L of isopropanol and then mixed with 10 μ L of streptavidin-coated SPA beads (20 mg/mL). The products were determined by Microbeta2 scintillation counter. Positive control was carried out under the same conditions with 6 μ L of water replacing the tested compound and negative control only contained PRMT1 and [3 H]SAM. Inhibition ratio is calculated by the following equation: inhibition % = $((P - A)/(P - N)) \times 100$, in which A is the remaining activity of tested group, P is positive control, and N is negative control.

6. IC₅₀ and n_H Determination. To measure the IC₅₀ and n_H, serial concentrations of the tested compound were tested against varied PRMTs. SPA assay was performed for PRMT1, PRMT5, and PRMT8 in the same way as the single-dose inhibition study with H4(1–20)_{BTN} as substrate. For the enzymes with R4 peptide (PRMT3 and PRMT6) or H3.3 protein (CARM1) as substrate, P81 filter paper binding assay^{41–43,48} was used. In this assay, the reaction was carried out as in SPA assay and quenched by applying 20 μ L of mixture on P81 filter paper disks. Then the disks were successively subjected to air-drying and wash (50 mM NaHCO₃ buffer, pH 9). The redried disks were submerged in liquid scintillation cocktail, and the Microbeta2 counter was used to quantify the products. The readout was plotted against concentration and then fitted with IC₅₀ equation modified with the Hill equation: $A = (1/(1 + ([I]/IC_{50})^{n_H}))$, in which n_H is the Hill coefficient, A is the remaining activity of tested group, and [I] is the compound concentration. For each reaction, the concentrations of [3 H]SAM and the substrate were set around the respective K_m values (which were predetermined).

7. Fluorescence Titration. The fluorescence intensity was measured using a Fluoro-Max 4 fluorimeter (Horiba Jobin Yvon). A 125 μ L mixture containing 0.6 μ M compound 50 and 30 μ M PRMT1 was added into a fluorescence cuvette (Hellma 105.253-QS) and incubated for 2 min. Then an increasing amount of compound 50 (0.6 μ M) was added to dilute the concentration of PRMT1 while keeping the reporter concentration constant. The fluorescence spectra of PRMT1 with decreased concentrations were taken. The fluorescence spectrum of compound 50 was also taken without addition of PRMT1. The excitation wavelength was set at 620 nm. The emission wavelength ranged from 650 to 750 nm, and the excitation and emission slit widths were both set at 5 nm bandpass. The fluorescence intensity data at 675 nm were plotted against PRMT1 concentration. Binding affinity K_d was calculated by fitting the data with the equation $y = 12570 + \Delta F/(1 + (K_d/x))$, in which y is the fluorescence intensity (FI) at various concentrations of PRMT1, 12570 is the FI of compound 50, ΔF is the increasing amplitude of FI when all the compound 50 is saturated by PRMT1, and x is the concentration of PRMT1.

8. Cell Viability Assay and Western Blot for Compound 50 Treated Leukemia Cells. Basically, the experiments were performed as reported.⁴¹ Briefly, the cell viability was measured by CellTiter-Glo viability kit (Promega, Madison WI). 1000 cells were seeded in individual wells of 96-well plates, with 100 μ L culture volume per well. All these leukemia cell lines were grown in RPMI medium plus 10% fetal bovine serum. Indicated concentrations of compound 50 or the same amount of DMSO were added to the culture. At 0, 24, and 48 h after the drug treatment, 100 μ L of CellTiter-Glo reagent was added to each well. Luminescence signals, which are proportional to viable cell numbers in each well, were measured by microplate reader (Biotek, Winooski, VT). For detection of total ADMA level in cells, 4×10^5 cells were cultured with indicated concentrations of 50 or DMSO. Cells extracts were harvested after 24 h of treatment and resolved by SDS–PAGE. Total protein arginine methylation level was determined by Western blotting of Asym 24 (Millipore) and D6H8 (Cell Signaling, Beverly, MA) antibodies.

9. Molecular Docking. The whole simulation was carried out with Discovery Studio 4.0.⁶⁴ Docking sites were defined by receptor cavities. Site 1 was chosen and the radius of the site sphere was increased to 17.3 Å (the site volume was increased to 1250.75 Å³) so that the sphere can cover both SAM and arginine binding sites. Both compound 50 and PRMT1_αX(–) were automatically prepared by the software before docking with the in-built CDOCKER protocol.

Ten poses of compound 50 with highest –CDOCKER_ENERGY were generated. Then the crystal structure of PRMT1 (PDB code 1OR8) together with the cocrystallized SAH was superimposed with PRMT1_αX(–) docked with conformer 1 of compound 50 to do the comparison. Other parameters were used with the default setting.

■ ASSOCIATED CONTENT

Supporting Information

Additional experimental and computational data. This material is available free of charge via the Internet at <http://pubs.acs.org>.

■ AUTHOR INFORMATION

Corresponding Authors

*M.H.: phone, 404-413-5566; fax, 404-413-5505; e-mail, mhenary1@gsu.edu.

*Y.G.Z.: phone, 706-542-0277; fax, 706-542-5358; e-mail, yzheng@uga.edu.

Notes

The authors declare no competing financial interest.

■ ACKNOWLEDGMENTS

This work was supported by NIH Grant R01GM086717 (Y.G.Z.) and a Brains and Behavior grant (M.H.). We thank the members of Zheng group for PRMT protein expression and histone peptide synthesis. E.A.O. was supported through a Graduate Fellowship through the Center for Diagnostics and Therapeutics.

■ REFERENCES

- (1) Zheng, Y. G.; Wu, J.; Chen, Z.; Goodman, M. Chemical regulation of epigenetic modifications: opportunities for new cancer therapy. *Med. Res. Rev.* **2008**, *28*, 645–687.
- (2) Ng, S. S.; Yue, W. W.; Oppermann, U.; Klose, R. J. Dynamic protein methylation in chromatin biology. *Cell. Mol. Life Sci.* **2009**, *66*, 407–422.
- (3) Wolf, S. S. The protein arginine methyltransferase family: an update about function, new perspectives and the physiological role in humans. *Cell. Mol. Life Sci.* **2009**, *66*, 2109–2121.
- (4) Bedford, M. T.; Clarke, S. G. Protein arginine methylation in mammals: who, what, and why. *Mol. Cell* **2009**, *33*, 1–13.
- (5) Bedford, M. T. Arginine methylation at a glance. *J. Cell Sci.* **2007**, *120*, 4243–4246.
- (6) Wei, H.; Mundade, R.; Lange, K. C.; Lu, T. Protein arginine methylation of non-histone proteins and its role in diseases. *Cell Cycle* **2014**, *13*, 32–41.
- (7) Yang, Y.; Bedford, M. T. Protein arginine methyltransferases and cancer. *Nat. Rev. Cancer* **2013**, *13*, 37–50.
- (8) Di Lorenzo, A.; Bedford, M. T. Histone arginine methylation. *FEBS Lett.* **2011**, *585*, 2024–2031.
- (9) Tang, J.; Frankel, A.; Cook, R. J.; Kim, S.; Paik, W. K.; Williams, K. R.; Clarke, S.; Herschman, H. R. PRMT1 is the predominant type I protein arginine methyltransferase in mammalian cells. *J. Biol. Chem.* **2000**, *275*, 7723–7730.
- (10) Nicholson, T. B.; Chen, T.; Richard, S. The physiological and pathophysiological role of PRMT1-mediated protein arginine methylation. *Pharmacol. Res.* **2009**, *60*, 466–474.
- (11) Iwasaki, H.; Yada, T. Protein arginine methylation regulates insulin signaling in L6 skeletal muscle cells. *Biochem. Biophys. Res. Commun.* **2007**, *364*, 1015–1021.
- (12) Wang, H.; Huang, Z.-Q.; Xia, L.; Feng, Q.; Erdjument-Bromage, H.; Strahl, B. D.; Briggs, S. D.; Allis, C. D.; Wong, J.; Tempst, P.; Zhang, Y. Methylation of histone H4 at arginine 3 facilitating transcriptional activation by nuclear hormone receptor. *Science* **2001**, *293*, 853–857.
- (13) Kwak, Y. T.; Guo, J.; Prajapati, S.; Park, K.-J.; Surabhi, R. M.; Miller, B.; Gehrig, P.; Gaynor, R. B. Methylation of SPT5 regulates its

interaction with RNA polymerase II and transcriptional elongation properties. *Mol. Cell* **2003**, *11*, 1055–1066.

(14) Adams, M. M.; Wang, B.; Xia, Z.; Morales, J. C.; Lu, X.; Donehower, L. A.; Bochar, D. A.; Elledge, S. J.; Carpenter, P. B. 53BP1 oligomerization is independent of its methylation by PRMT1. *Cell Cycle* **2005**, *4*, 1854–1861.

(15) Bouras, G.; Deftereos, S.; Tousoulis, D.; Giannopoulos, G.; Chatzis, G.; Tsounis, D.; W. Cleman, M.; Stefanadis, C. Asymmetric dimethylarginine (ADMA): a promising biomarker for cardiovascular disease? *Curr. Top. Med. Chem.* **2013**, *13*, 180–200.

(16) Osanai, T.; Saitoh, M.; Sasaki, S.; Tomita, H.; Matsunaga, T.; Okumura, K. Effect of shear stress on asymmetric dimethylarginine release from vascular endothelial cells. *Hypertension* **2003**, *42*, 985–990.

(17) Böger, R. H.; Sydow, K.; Borlak, J.; Thum, T.; Lenzen, H.; Schubert, B.; Tsikas, D.; Bode-Böger, S. M. LDL cholesterol upregulates synthesis of asymmetrical dimethylarginine in human endothelial cells: involvement of S-adenosylmethionine-dependent methyltransferases. *Circ. Res.* **2000**, *87*, 99–105.

(18) Matsuguma, K.; Ueda, S.; Yamagishi, S.-i.; Matsumoto, Y.; Kaneyuki, U.; Shibata, R.; Fujimura, T.; Matsuoka, H.; Kimoto, M.; Kato, S.; Imaizumi, T.; Okuda, S. Molecular mechanism for elevation of asymmetric dimethylarginine and its role for hypertension in chronic kidney disease. *J. Am. Soc. Nephrol.* **2006**, *17*, 2176–2183.

(19) Cvetković, T.; Pavlović, R.; Đorđević, V.; Stojanović, I.; Veličković-Radovanović, R.; Ignjatović, A.; Stefanović, N.; Živanović, S.; Đorđević, V. Dimethylarginine—biomarkers in progression of kidney disease. *J. Med. Biochem.* **2012**, *31*, 301–308.

(20) Leone, A.; Moncada, S.; Vallance, P.; Calver, A.; Collier, J. Accumulation of an endogenous inhibitor of nitric oxide synthesis in chronic renal failure. *Lancet* **1992**, *339*, 572–575.

(21) Raptis, V.; Kapoulas, S.; Grekas, D. Role of asymmetrical dimethylarginine in the progression of renal disease. *Nephrology* **2013**, *18*, 11–21.

(22) Ueda, S.; Yamagishi, S.-I.; Kaida, Y.; Okuda, S. Asymmetric dimethylarginine may be a missing link between cardiovascular disease and chronic kidney disease. *Nephrology* **2007**, *12*, 582–590.

(23) Seligson, D. B.; Horvath, S.; Shi, T.; Yu, H.; Tze, S.; Grunstein, M.; Kurdistani, S. K. Global histone modification patterns predict risk of prostate cancer recurrence. *Nature* **2005**, *435*, 1262–1266.

(24) Le Romancer, M.; Treilleux, I.; Boucheikoua-Bouzaghrou, K.; Sentis, S.; Corbo, L. Methylation, a key step for nongenomic estrogen signaling in breast tumors. *Steroids* **2010**, *75*, 560–564.

(25) Cheung, N.; Chan, L. C.; Thompson, A.; Cleary, M. L.; So, C. W. E. Protein arginine-methyltransferase-dependent oncogenesis. *Nat. Cell Biol.* **2007**, *9*, 1208–1215.

(26) Shia, W.-J.; Okumura, A. J.; Yan, M.; Sarkeshik, A.; Lo, M.-C.; Matsuura, S.; Komeno, Y.; Zhao, X.; Nimer, S. D.; Yates, J. R.; Zhang, D.-E. PRMT1 interacts with AML1-ETO to promote its transcriptional activation and progenitor cell proliferative potential. *Blood* **2012**, *119*, 4953–4962.

(27) 't Hart, P.; Thomas, D.; van Ommeren, R.; Lakowski, T. M.; Frankel, A.; Martin, N. I. Analogues of the HIV-Tat peptide containing N[small eta]-modified arginines as potent inhibitors of protein arginine N-methyltransferases. *MedChemComm* **2012**, *3*, 1235–1244.

(28) Obianyo, O.; Causey, C. P.; Osborne, T. C.; Jones, J. E.; Lee, Y.-H.; Stallcup, M. R.; Thompson, P. R. A chloroacetamide-based inactivator of protein arginine methyltransferase 1: design, synthesis, and in vitro and in vivo evaluation. *ChemBioChem* **2010**, *11*, 1219–1223.

(29) Osborne, T.; Weller Roska, R. L.; Rajski, S. R.; Thompson, P. R. In situ generation of a bisubstrate analogue for protein arginine methyltransferase 1. *J. Am. Chem. Soc.* **2008**, *130*, 4574–4575.

(30) Wahle, E.; Moritz, B. Methylation of the nuclear poly(A)-binding protein by type I protein arginine methyltransferases—how and why. *Biol. Chem.* **2013**, *394*, 1029–1043.

(31) Cha, B.; Jho, E.-H. Protein arginine methyltransferases (PRMTs) as therapeutic targets. *Expert Opin. Ther. Targets* **2012**, *16*, 651–664.

(32) Spannhoff, A.; Machmur, R.; Heinke, R.; Trojer, P.; Bauer, I.; Brosch, G.; Schüle, R.; Hanefeld, W.; Sippl, W.; Jung, M. A novel arginine methyltransferase inhibitor with cellular activity. *Bioorg. Med. Chem. Lett.* **2007**, *17*, 4150–4153.

(33) Spannhoff, A.; Heinke, R.; Bauer, I.; Trojer, P.; Metzger, E.; Gust, R.; Schüle, R.; Brosch, G.; Sippl, W.; Jung, M. Target-based approach to inhibitors of histone arginine methyltransferases. *J. Med. Chem.* **2007**, *50*, 2319–2325.

(34) Ragno, R.; Simeoni, S.; Castellano, S.; Vicidomini, C.; Mai, A.; Caroli, A.; Tramontano, A.; Bonaccini, C.; Trojer, P.; Bauer, I.; Brosch, G.; Sbardella, G. Small molecule inhibitors of histone arginine methyltransferases: homology modeling, molecular docking, binding mode analysis, and biological evaluations. *J. Med. Chem.* **2007**, *50*, 1241–1253.

(35) Cheng, D.; Yadav, N.; King, R. W.; Swanson, M. S.; Weinstein, E. J.; Bedford, M. T. Small molecule regulators of protein arginine methyltransferases. *J. Biol. Chem.* **2004**, *279*, 23892–23899.

(36) Fontán, N.; García-Domínguez, P.; Álvarez, R.; de Lera, Á. R. Novel symmetrical ureas as modulators of protein arginine methyltransferases. *Bioorg. Med. Chem.* **2013**, *21*, 2056–2067.

(37) Dowden, J.; Pike, R. A.; Parry, R. V.; Hong, W.; Muhsen, U. A.; Ward, S. G. Small molecule inhibitors that discriminate between protein arginine N-methyltransferases PRMT1 and CARM1. *Org. Biomol. Chem.* **2011**, *9*, 7814–7821.

(38) Bissinger, E.-M.; Heinke, R.; Spannhoff, A.; Eberlin, A.; Metzger, E.; Cura, V.; Hassenboehler, P.; Cavarelli, J.; Schüle, R.; Bedford, M. T.; Sippl, W.; Jung, M. Acyl derivatives of *p*-aminosulfonamides and dapsone as new inhibitors of the arginine methyltransferase hPRMT1. *Bioorg. Med. Chem.* **2011**, *19*, 3717–3731.

(39) Castellano, S.; Milite, C.; Ragno, R.; Simeoni, S.; Mai, A.; Limongelli, V.; Novellino, E.; Bauer, I.; Brosch, G.; Spannhoff, A.; Cheng, D.; Bedford, M. T.; Sbardella, G. Design, synthesis and biological evaluation of carboxy analogues of arginine methyltransferase inhibitor 1 (AMI-1). *ChemMedChem* **2010**, *5*, 398–414.

(40) Heinke, R.; Spannhoff, A.; Meier, R.; Trojer, P.; Bauer, I.; Jung, M.; Sippl, W. Virtual screening and biological characterization of novel histone arginine methyltransferase PRMT1 inhibitors. *ChemMedChem* **2009**, *4*, 69–77.

(41) Yan, L.; Yan, C.; Qian, K.; Su, H.; Kofsky-Wofford, S. A.; Lee, W.-C.; Zhao, X.; Ho, M.-C.; Ivanov, I.; Zheng, Y. G. Diamidine compounds for selective inhibition of protein arginine methyltransferase 1. *J. Med. Chem.* **2014**, *57*, 2611–2622.

(42) Wang, J.; Chen, L.; Sinha, S. H.; Liang, Z.; Chai, H.; Muniyan, S.; Chou, Y.-W.; Yang, C.; Yan, L.; Feng, Y.; Li, K. K.; Lin, M.-F.; Jiang, H.; Zheng, Y. G.; Luo, C. Pharmacophore-based virtual screening and biological evaluation of small molecule inhibitors for protein arginine methylation. *J. Med. Chem.* **2012**, *55*, 7978–7987.

(43) Feng, Y.; Li, M.; Wang, B.; Zheng, Y. G. Discovery and mechanistic study of a class of protein arginine methylation inhibitors. *J. Med. Chem.* **2010**, *53*, 6028–6039.

(44) Castellano, S.; Spannhoff, A.; Milite, C.; Dal Piaz, F.; Cheng, D.; Tosco, A.; Viviano, M.; Yamani, A.; Cianciulli, A.; Sala, M.; Cura, V.; Cavarelli, J.; Novellino, E.; Mai, A.; Bedford, M. T.; Sbardella, G. Identification of small-molecule enhancers of arginine methylation catalyzed by coactivator-associated arginine methyltransferase 1. *J. Med. Chem.* **2012**, *55*, 9875–9890.

(45) Patonay, G.; Salon, J.; Sowell, J.; Strekowski, L. Noncovalent labeling of biomolecules with red and near-infrared dyes. *Molecules* **2004**, *9*, 40–49.

(46) Narayanan, N.; Patonay, G. A new method for the synthesis of heptamethine cyanine dyes: synthesis of new near-infrared fluorescent labels. *J. Org. Chem.* **1995**, *60*, 2391–2395.

(47) Flanagan, J. H.; Khan, S. H.; Menchen, S.; Soper, S. A.; Hammer, R. P. Functionalized tricyanin dyes as near-infrared fluorescent probes for biomolecules. *Bioconjugate Chem.* **1997**, *8*, 751–756.

(48) Sinha, S. H.; Owens, E. A.; Feng, Y.; Yang, Y.; Xie, Y.; Tu, Y.; Henary, M.; Zheng, Y. G. Synthesis and evaluation of carbocyanine

- dyes as PRMT inhibitors and imaging agents. *Eur. J. Med. Chem.* **2012**, *54*, 647–659.
- (49) Davidson, Y. Y.; Gunn, B. M.; Soper, S. A. Spectroscopic and binding properties of near-infrared tricyanocyanine dyes to double-stranded DNA. *Appl. Spectrosc.* **1996**, *50*, 211–221.
- (50) Seifert, J. L.; Connor, R. E.; Kushon, S. A.; Wang, M.; Armitage, B. A. Spontaneous assembly of helical cyanine dye aggregates on DNA nanotemplates. *J. Am. Chem. Soc.* **1999**, *121*, 2987–2995.
- (51) Wang, M.; Silva, G. L.; Armitage, B. A. DNA-templated formation of a helical cyanine dye J-aggregate. *J. Am. Chem. Soc.* **2000**, *122*, 9977–9986.
- (52) Wu, J.; Xie, N.; Feng, Y.; Zheng, Y. G. Scintillation proximity assay of arginine methylation. *J. Biomol. Screening* **2012**, *17*, 237–244.
- (53) Hernandez, M. Z.; Cavalcanti, S. M.; Moreira, D. R.; de Azevedo Junior, W. F.; Leite, A. C. Halogen atoms in the modern medicinal chemistry: hints for the drug design. *Curr. Drug Targets* **2010**, *11*, 303–314.
- (54) Wilcken, R.; Zimmermann, M. O.; Lange, A.; Joerger, A. C.; Boeckler, F. M. Principles and applications of halogen bonding in medicinal chemistry and chemical biology. *J. Med. Chem.* **2012**, *56*, 1363–1388.
- (55) Nanjunda, R.; Owens, E.; Mickelson, L.; Dost, T.; Stroeve, E.; Huynh, H.; Germann, M.; Henary, M.; Wilson, W. Selective G-quadruplex DNA recognition by a new class of designed cyanines. *Molecules* **2013**, *18*, 13588–13607.
- (56) Nanjunda, R.; Owens, E. A.; Mickelson, L.; Alyabyev, S.; Kilpatrick, N.; Wang, S.; Henary, M.; Wilson, W. D. Halogenated pentamethine cyanine dyes exhibiting high fidelity for G-quadruplex DNA. *Bioorg. Med. Chem.* **2012**, *20*, 7002–7011.
- (57) Shoichet, B. K. Interpreting steep dose-response curves in early inhibitor discovery. *J. Med. Chem.* **2006**, *49*, 7274–7277.
- (58) Zhang, X.; Cheng, X. Structure of the predominant protein arginine methyltransferase PRMT1 and analysis of its binding to substrate peptides. *Structure* **2003**, *11*, 509–520.
- (59) Gesztelyi, R.; Zsuga, J.; Kemeny-Beke, A.; Varga, B.; Juhasz, B.; Tosaki, A. The Hill equation and the origin of quantitative pharmacology. *Arch. Hist. Exact Sci.* **2012**, *66*, 427–438.
- (60) McGovern, S. L.; Caselli, E.; Grigorieff, N.; Shoichet, B. K. A common mechanism underlying promiscuous inhibitors from virtual and high-throughput screening. *J. Med. Chem.* **2002**, *45*, 1712–1722.
- (61) Seidler, J.; McGovern, S. L.; Doman, T. N.; Shoichet, B. K. Identification and prediction of promiscuous aggregating inhibitors among known drugs. *J. Med. Chem.* **2003**, *46*, 4477–4486.
- (62) Straus, O. H.; Goldstein, A.; Plachte, W. t. T. A. o. F. L. Zone behavior of enzymes: illustrated by the effect of dissociation constant and dilution on the system cholinesterase-physostigmine. *J. Gen. Physiol.* **1943**, *26*, 559–585.
- (63) Selvi, B. R.; Batta, K.; Kishore, A. H.; Mantelingu, K.; Varier, R. A.; Balasubramanyam, K.; Pradhan, S. K.; Dasgupta, D.; Sriram, S.; Agrawal, S.; Kundu, T. K. Identification of a novel inhibitor of coactivator-associated arginine methyltransferase 1 (CARM1)-mediated methylation of histone H3 Arg-17. *J. Biol. Chem.* **2010**, *285*, 7143–7152.
- (64) Martin, N. I.; Liskamp, R. M. J. Preparation of NG-substituted L-arginine analogues suitable for solid phase peptide synthesis. *J. Org. Chem.* **2008**, *73*, 7849–7851.
- (65) Zhang, X.; Zhou, L.; Cheng, X. Crystal structure of the conserved core of protein arginine methyltransferase PRMT3. *EMBO J.* **2000**, *19*, 3509–3519.
- (66) Troffer-Charlier, N.; Cura, V.; Hassenboehler, P.; Moras, D.; Cavarelli, J. Functional insights from structures of coactivator-associated arginine methyltransferase 1 domains. *EMBO J.* **2007**, *26*, 4391–4401.
- (67) Yue, W. W.; Hassler, M.; Roe, S. M.; Thompson-Vale, V.; Pearl, L. H. Insights into histone code syntax from structural and biochemical studies of CARM1 methyltransferase. *EMBO J.* **2007**, *26*, 4402–4412.
- (68) Wang, C.; Zhu, Y.; Chen, J.; Li, X.; Peng, J.; Chen, J.; Zou, Y.; Zhang, Z.; Jin, H.; Yang, P.; Wu, J.; Niu, L.; Gong, Q.; Teng, M.; Shi, Y. Crystal structure of arginine methyltransferase 6 from *Trypanosoma brucei*. *PLoS One* **2014**, *9*, e87267.
- (69) Rust, H. L.; Zurita-Lopez, C. I.; Clarke, S.; Thompson, P. R. Mechanistic studies on transcriptional coactivator protein arginine methyltransferase 1. *Biochemistry* **2011**, *50*, 3332–3345.
- (70) Gary, J. D.; Clarke, S. RNA and protein interactions modulated by protein arginine methylation. *Prog. Nucleic Acid Res. Mol. Biol.* **1998**, *61*, 65–131.
- (71) Lee, J.; Bedford, M. T. PABP1 identified as an arginine methyltransferase substrate using high-density protein arrays. *EMBO Rep.* **2002**, *3*, 268–273.
- (72) Ferguson, A. D.; Larsen, N. A.; Howard, T.; Pollard, H.; Green, I.; Grande, C.; Cheung, T.; Garcia-Arenas, R.; Cowen, S.; Wu, J.; Godin, R.; Chen, H.; Keen, N. Structural basis of substrate methylation and inhibition of SMYD2. *Structure* **2011**, *19*, 1262–1273.
- (73) Liu, F.; Chen, X.; Allali-Hassani, A.; Quinn, A. M.; Wasney, G. A.; Dong, A.; Barsyte, D.; Kozieradzki, I.; Senisterra, G.; Chau, I.; Sierheyeva, A.; Kireev, D. B.; Jadhav, A.; Herold, J. M.; Frye, S. V.; Arrowsmith, C. H.; Brown, P. J.; Simeonov, A.; Vedadi, M.; Jin, J. Discovery of a 2,4-diamino-7-aminoalkoxyquinazoline as a potent and selective inhibitor of histone lysine methyltransferase G9a. *J. Med. Chem.* **2009**, *52*, 7950–7953.
- (74) Vedadi, M.; Barsyte-Lovejoy, D.; Liu, F.; Rival-Gervier, S.; Allali-Hassani, A.; Labrie, V.; Wigle, T. J.; DiMaggio, P. A.; Wasney, G. A.; Sierheyeva, A.; Dong, A.; Tempel, W.; Wang, S.-C.; Chen, X.; Chau, I.; Mangano, T. J.; Huang, X.-p.; Simpson, C. D.; Pattenden, S. G.; Norris, J. L.; Kireev, D. B.; Tripathy, A.; Edwards, A.; Roth, B. L.; Janzen, W. P.; Garcia, B. A.; Petronis, A.; Ellis, J.; Brown, P. J.; Frye, S. V.; Arrowsmith, C. H.; Jin, J. A chemical probe selectively inhibits G9a and GLP methyltransferase activity in cells. *Nat. Chem. Biol.* **2011**, *7*, 566–574.
- (75) Chang, Y.; Ganesh, T.; Horton, J. R.; Spannhoff, A.; Liu, J.; Sun, A.; Zhang, X.; Bedford, M. T.; Shinkai, Y.; Snyder, J. P.; Cheng, X. Adding a lysine mimic in the design of potent inhibitors of histone lysine methyltransferases. *J. Mol. Biol.* **2010**, *400*, 1–7.
- (76) Xie, N.; Elangwe, E. N.; Asher, S.; Zheng, Y. G. A dual-mode fluorescence strategy for screening HAT modulators. *Bioconjugate Chem.* **2009**, *20*, 360–366.
- (77) Feng, Y.; Xie, N.; Wu, J.; Yang, C.; Zheng, Y. G. Inhibitory study of protein arginine methyltransferase 1 using a fluorescent approach. *Biochem. Biophys. Res. Commun.* **2009**, *379*, 567–572.
- (78) Feng, Y.; Xie, N.; Jin, M.; Stahley, M. R.; Stivers, J. T.; Zheng, Y. G. A transient kinetic analysis of PRMT1 catalysis. *Biochemistry* **2011**, *50*, 7033–7044.
- (79) Feng, Y.; Wang, J.; Asher, S.; Hoang, L.; Guardiani, C.; Ivanov, I.; Zheng, Y. G. Histone H4 acetylation differentially modulates arginine methylation by an in cis mechanism. *J. Biol. Chem.* **2011**, *286*, 20323–20334.